Summer 7-27-2012

A Hybrid Battery Model Capable of Capturing Dynamic Circuit Characteristics and Nonlinear Capacity Effects

Taesic Kim
University of Nebraska-Lincoln, taesickim@huskers.unl.edu

A Hybrid Battery Model Capable of Capturing Dynamic Circuit Characteristics and Nonlinear Capacity Effects

By

Taesic Kim

Presented to the Faculty of

The Graduate College at the University of Nebraska

In Partial Fulfillment of Requirements

For the Degree of Master of Science

Major: Electrical Engineering

Under the Supervision of Professor Wei Qiao

Lincoln, Nebraska

July, 2012

A Hybrid Battery Model Capable of Capturing Dynamic Circuit Characteristics and Nonlinear Capacity Effects

Taesic Kim, M.S.

University of Nebraska, 2012

Adviser: Wei Qiao

A high-fidelity battery model capable of accurately predicting battery performance is required for proper design and operation of battery-powered systems. However, the existing battery models have at least one of the following drawbacks: 1) requiring intensive computation due to high complexity, 2) not applicable for electrical circuit design and simulation, and 3) not capable of accurately capturing the State of Charge (SOC) and predicting runtime of the battery due to neglecting the nonlinear capacity effects. This thesis proposes a novel hybrid battery model, which takes the advantages of an electrical circuit battery model to accurately predicting the dynamic circuit characteristics of the battery, and an analytical battery model to capturing the nonlinear capacity effects for accurate SOC tracking and runtime prediction of the battery. The proposed battery model is validated by simulation and experimental studies for single-cell and multicell polymer lithium-ion batteries as well as for a lead-acid battery. The proposed model is applicable to other types and sizes of electrochemical battery cells, such as Nikel Cadmium (NiCd) and Nikel Metal Hydride (NiMH). The proposed battery model is computationally effective for simulation, design, and real-time management of battery-powered systems.

This thesis is based upon work supported by the U.S. National Science Foundation under CAREER Award ECCS-0954938. Any findings, opinions, and conclusions or recommendations expressed in this thesis are those of the author and do not necessarily reflect the views of the National Science Foundation.

Acknowledgements

First of all, I would like to give my sincere appreciation and great gratitude to my advisor, Dr. Wei Qiao, for his encouragement and assistance in the technical and personal aspects of my graduate study as well as constructive review and comments to my thesis.

I am grateful to Dr. Liyan Qu, and my committee members, Drs. Jerry L. Hudgins and Sohrab Asgarpoor, for their valuable reviews to my thesis and cheerful comments and considerations to me.

I am also grateful to all of my colleagues in the Power & Energy Systems Laboratory for their friendship and technical insight.

I would also give my thanks to my congress members in Korea Church of Lincoln and all my friends in Lincoln.

Finally, I would like to thank my wife, Dr. Jeongsoon Lee, for her steadfast devotion, love, and encouragement toward me. Thanks my lovely daughter, Dana. She is the gift giving me happiness and reminding me grace from God.

Table of Contents

List of Acronyms

A-h	ampere-hours
ANN	artificial neural network
CCCV	constant current constant voltage
C.C.	constant current
C.R.	constant resistor
DOD	depth of discharge
EIS	electrochemical impedance spectroscopy
EKF	extended Kalman filter
I-V	current-voltage
KiBaM	kinetic battery model
LSD NiMH	low self-discharge nickel metal hydride
NiCd	nickel cadmium
NiMH	nickel metal hydride
P.C.	pulse current
PCB	printed circuit board
RNN	recurrent neural network
SOC	state of charge
SOH	state of health

List of Figures

List of Tables

Chapter 1: Introduction

1.1 Motivation of the Work

Rechargeable batteries have been more and more pervasively used as the energy storage and power source for various electrical systems and devices, such as communication systems, electronic devices, renewable power systems, electric vehicles, etc. The proper design and operation of these battery-powered systems and devices requires an appropriate battery model. For example, modern battery power management systems rely on a high-fidelity battery model to track the State of Charge (SOC) and predict runtime of each battery cell and the whole battery system to optimize its performance. This requires the battery model can accurately capture various nonlinear capacity effects of the battery. Moreover, the proper design of a battery-powered electrical system or device requires the battery model to be capable of accurately capturing the dynamic electrical circuit characteristics of the battery to facilitate the system-level circuit design and simulation.

1.2 Overview of Rechargeable Battery Characteristics

1.2.1 Capacity

Capacity is the amount of electric charge that a battery can store, which is measured in a unit of Ampere-hours (A-h). This A-h unit represents the amount of electricity that a battery can deliver at one Ampere during one hour, and the battery capacity represents the maximum amount of energy that can be drawn from a fully charged battery until its terminal voltage reaches the cutoff value (i.e., the fully discharged

condition). The C rating is specified as the capacity for a given time of discharge. For example, theoretically, a battery with a rated capacity of 2 A-h will be discharged for 2 hours at 1 A (i.e., 0.5C) from the fully charged condition to the fully discharged condition. However, the actual capacity of a battery can vary significantly from the rated capacity due to the nonlinear capacity effects resulting from past charges and discharges, aging of the battery, charging or discharging regime of the battery, ambient temperature, etc.

1.2.2 State of Charge

SOC is defined as the percentage of the available capacity ($C_{available}$) with respect to the maximum available capacity (C_{max}) of a battery. For example, if a battery is fully charged, its SOC is 100%. On the other hand, a 0% SOC means that the battery is fully discharged. A variety of battery SOC estimation methods have been developed, which, in general, can be classified into four categories: Coulomb counting methods, computational intelligence-based methods, model-based methods, and mixed methods. The Coulomb counting methods are simple and easy to implement in real-time systems [1]. In these methods, the SOC is simply calculated by integrating the measured current over time with the information of the initial SOC ($SOC_{initial}$).

$$SOC(t) = \frac{C_{available}(t)}{C_{\max}} = SOC_{initial} - \frac{\int i_{cell}(t)}{C_{\max}} \tag{1-1}$$

However, the Coulomb counting methods have unrecoverable problems that might be caused by factors such as a wrong initial SOC value and accumulation of estimation errors. Moreover, the Coulomb counting methods cannot keep track battery nonlinear capacity variation effects, such as the rate capacity effect and recovery effect.

The computational intelligence-based methods describe the nonlinear relationship between the SOC of a battery and the factors influencing the SOC, such as battery voltage, current, and temperature. Artificial neural network (ANN)-based models [2], [3], fuzzy logic models [4], [5], support vector regression models [6], and mixed models have been used to estimate the SOC of a battery [7]. Figure 1 illustrates a typical three-layer feedforward ANN architecture used for battery modeling. The ANN consists of one input layer, one hidden layer, and one output layer. The input layer consists of voltage, current, and a bias 1. Five neurons with sigmoidal activation functions are used in the hidden layer. The ANN outputs SOC value at the output layer. Wij (i = 1, ⋯, 5; j = 1, 2, 3) and Vij (i = 1; j = 1, ⋯, 6) are the weights between input and hidden layers and the weights between hidden and output layers, respectively. Although accurate SOC estimation of a battery can be obtained from the computational intelligence-based methods by including the nonlinearity of the battery, the learning process required by these methods has a quite high computational cost and is difficult to implement for real-time SOC tracking.

Model-based SOC estimation methods basically utilize state-space electrical battery models to design an observer for real-time SOC estimation. For example, Kalman filter [8] and extended Kalman filter (EKF) [9]-[11] have been used to estimate the SOC of a battery based on the electrical circuit model of the battery for hybrid electric vehicle and electric vehicle applications. However, these methods require an accurate electrical battery model and higher computation cost than the nonmodel-based Coulomb counting methods. Furthermore, the estimation error can be large when unexpected noise is present [12].

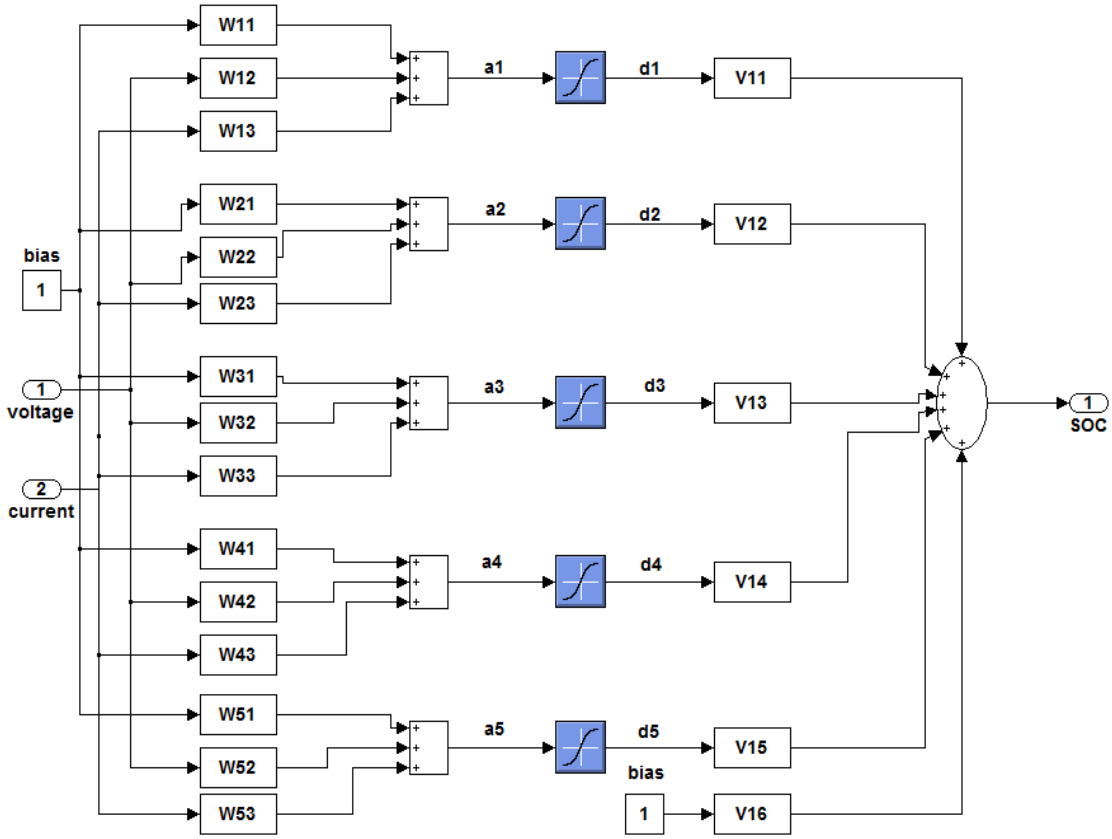

Figure 1. A typical three-layer feedforward ANN used for battery modeling.

The mixed SOC estimation methods combine the advantages of the aforementioned three methods [13]. In [13], the SOC of lithium-ion batteries are estimated by using neural networks and EKF.

1.2.3 Nonlinear Capacity Effects in Discharge

The two important effects that influence battery discharge performance sensitively are rate capacity effect and recovery effect. Both of them are called nonlinear capacity effects.

An electrochemical battery cell essentially consists of an anode (i.e., negative electrode) and a cathode (i.e., positive electrode) placed in an electrolyte medium. The electrolyte with a separator separates the two electrodes, as shown in Figure 2 [14]. The electrical current obtained from a cell results from electrochemical reactions, causing the extraction of electrons at the anode and injection of electrons at the cathode. For example, a lithium-ion cell has $LiCoO_2$ as the positive electrode material and Li_xC_6 as the negative electrode material. The electrochemical reactions during discharge are expressed as follows [14].

$$\begin{aligned} cathod &: Li_{1-x}CoO_2 + xLi^+ + xe^- \rightarrow LiCoO_2 \\ anode &: Li_xC_6 - xe^- \rightarrow 6C + xLi^+ \end{aligned} \tag{1-2}$$

The process will be reversed during charge.

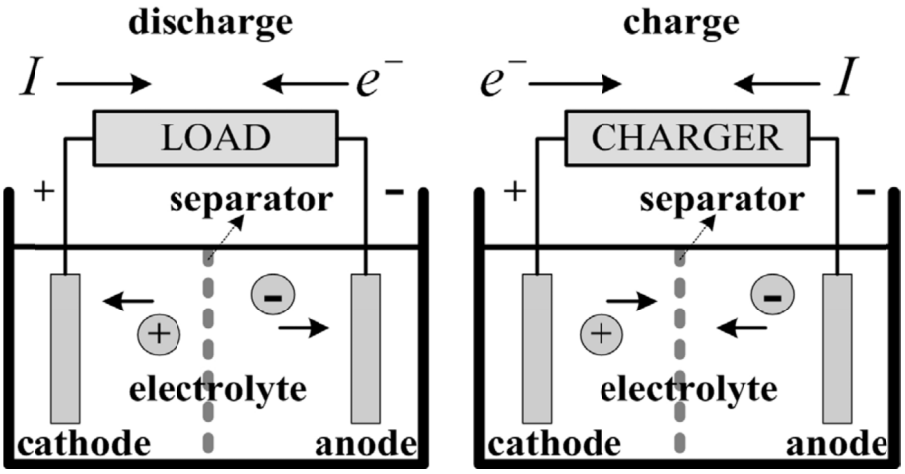

Figure 2. Configuration and operating principle of an electrochemical battery. (Courtesy of [14].)

A simplified expression for the electrochemical reactions, involving electrons e^-, oxidized species O (e.g., Li^+), and reduced species R, can be described as follows [15]:

$$\begin{aligned} cathod &: O + e^{-} \rightarrow R \\ anode &: R - e^{-} \rightarrow O \end{aligned} \tag{1-3}$$

The gain of electrons at the cathode (oxidation) is coupled with the loss of electrons at the anode (reduction). Assuming that an electrochemical battery is symmetric and the two electrodes react similarly, only species *O* and the cathode can be considered to express discharge behavior of the battery.

The concentration of species *O* with respect to position is illustrated in Figure 3. At the initial state, the species *O* are uniformly distributed inside the battery. Once the battery is discharged, the species *O* at the cathode accept electrons from the external circuit and the species *R*. This causes reduction of *O* near the cathode, resulting in a concentration gradient of *O* across the battery. Due to this gradient, the species *O* that are further away from the cathode diffuse to the cathode. When the battery is discharged at a low current, the diffusion tends to increase the concentration of *O* at the cathode. Eventually, the diffusion and the consumption reach a balance at the cathode, and the overall concentration of *O* at the cathode keeps dropping. Once the concentration falls below a certain level or reaches the bottom, the battery will fail to operate (i.e., the battery is fully discharged). As the current is increased, the gradient of the concentration becomes more significant and the available capacity as well as the cell voltage decrease faster. This important phenomenon is named the rate capacity effect [16]. Figure 4 shows that the effective available capacity drops and changes the battery voltage with increasing discharge current for a polymer lithium-ion battery cell [17].

If the battery is allowed to rest for enough time (i.e., switching off in Figure 3), the reaction of transformation at the cathode from species *O* to species *R* stops. However, the

gradient of concentration inside the battery still exists and the diffusion will continue until the gradient of concentration disappears. Therefore, the reduced available capacity due to the rate capacity effect is recovered. This nonlinear behavior is called the recovery effect [18] and is shown in Figure 5. The off-time is not shown in Figure 5 in order to compare the increased gain in terms of operating time obtained in the intermittent discharge with the constant discharge. The recovery effect typically depends on the rate of the discharge current, SOC, rest time, and battery construction [18].

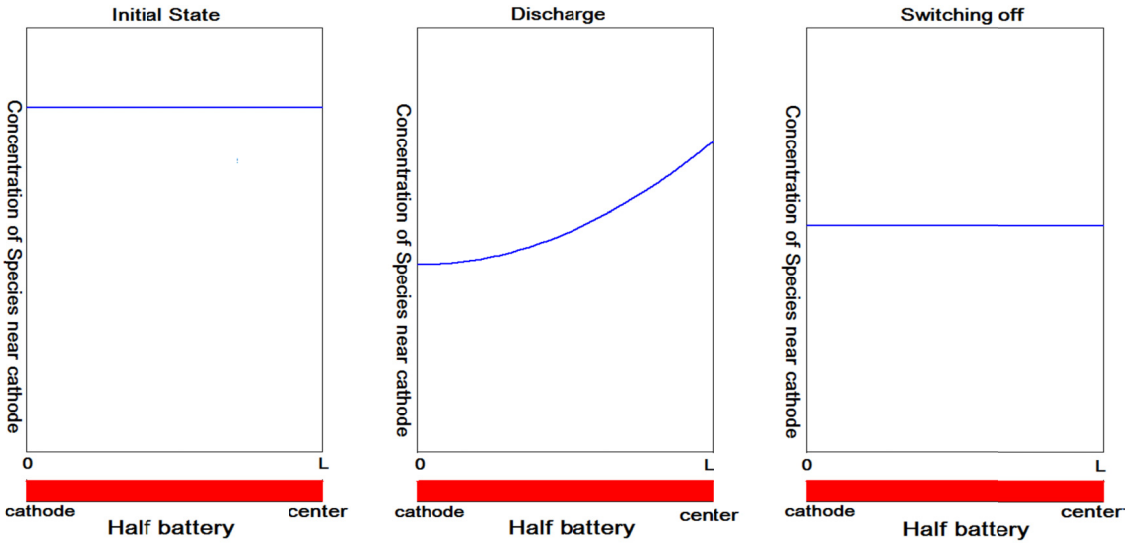

Figure 3. Concentration of species *O* near the cathode: Left, before discharge; middle, during discharge; right, after discharge. (Courtesy of [15].)

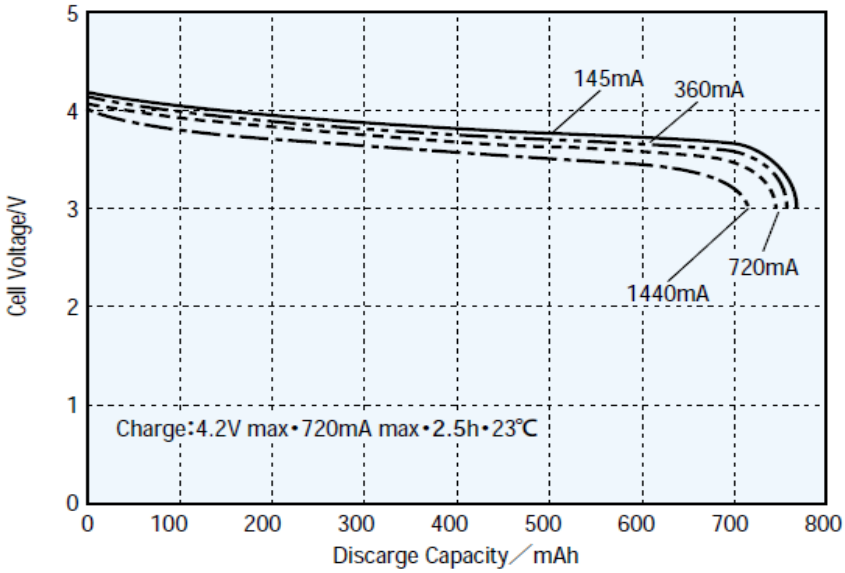

Figure 4. Rate capacity effect of a polymer lithium-ion battery cell: effective discharge (available) capacity drops and changes battery voltage with the discharge current at 145 mA, 360 mA, 720 mA, and 1440 mA at an ambient temperature of 23°C. (Courtesy of [17].)

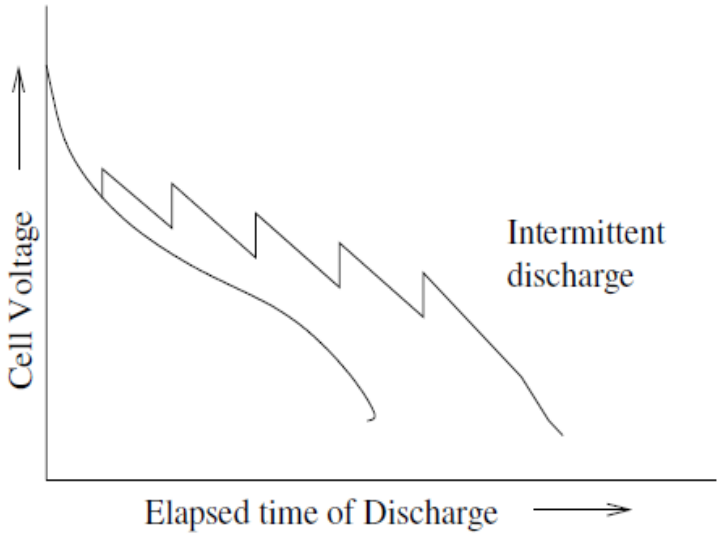

Figure 5. Recovery effect: (battery) cell voltage as the results of constant and intermittent discharges. (Courtesy of [18].)

1.2.4 Charging Process

During the charging process the energy that has been discharged from the battery is recovered. Figure 6 shows the voltage, current, and capacity of a lithium-ion battery

when it is being charged under Constant Current Constant Voltage (CCCV) conditions, where the maximum charging voltage is 4.2V, the maximum charging current is 720 mA, and the ambient temperature is 23°C [17].

The charging process also has nonlinear characteristics based on the SOC, charge current rate, and temperature [19]. Once a battery is fully charged (i.e., SOC = 100 %) or its voltage is over the maximum charge voltage (V_{max}), the charging current becomes dissipated, resulting in the generation of heat and gasses. If the battery is overcharged, the elevated temperature boils and dries the electrolyte as well as vents or bursts the battery. These may cause permanent damage of the battery.

A high charge current rate reduces the charge efficiency due to the limit of the charge acceptance rate and the heat dissipation. For example, in a lithium-ion battery cell there is a limitation for lithium-ions to go into the layers of the anode due to the chemical reaction time (i.e., the diffusion process or mass transport). Too much charge current through the battery will cause surplus ions being deposited on the anode in the form of lithium metal. This will result in an irreversible capacity loss. Continuing to charge a battery with a high current rate can cause local overcharge, polarization, overheating, and unwanted chemical reaction, resulting in damage of the battery. This also causes the terminals of the battery to quickly reach a very high voltage, indicating that the battery has been fully charged. As mentioned before, charge acceptance rate can be recovered if the battery is allowed to relax [20] or if the proper instantaneous discharge with the reverse large current is used instead of relax during charge [21].

Ambient temperature significantly influences the charge acceptance and charge time as well. Lower temperature reduces charge acceptance and increases charge time [19].

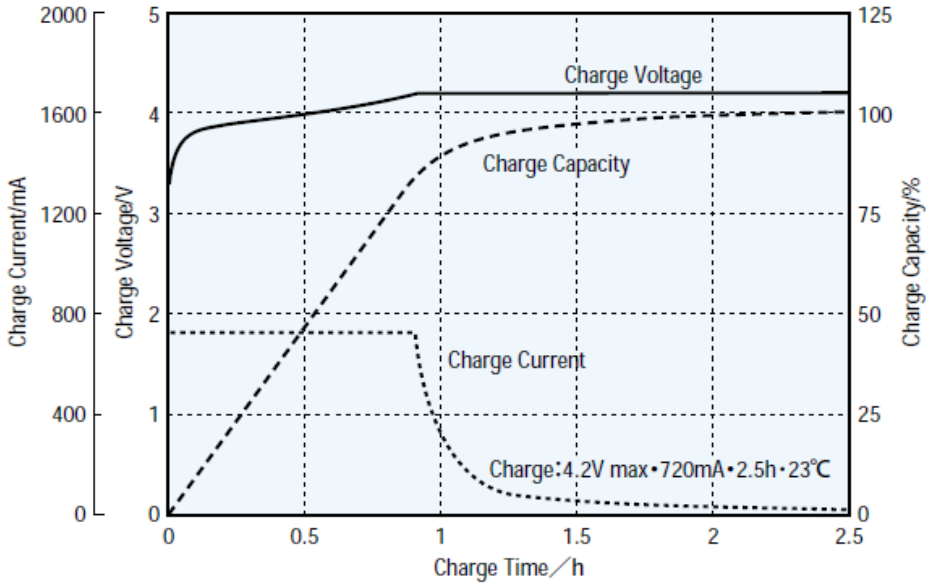

Figure 6. The voltage, current, and capacity of a lithium-ion battery when it is being charged under CCCV conditions. (Courtesy of [17].)

1.2.5 Temperature Effect

Battery operation has a strongly dependency on temperature, which is a crucial factor for safety consideration. Figure 7 shows changes in the discharge voltage of a polymer lithium-ion battery cell for a constant discharge current of 360 mA at ambient temperatures of -20°C, -10°C, 0°C, 23°C, and 45°C [17]. Below the room temperature (e.g., < 23°C), the chemical reactions in the battery decreases and the internal resistance increases, which cause the reduction of the full charge capacity and increase of the slope of the discharge voltage curve. On the other hand, at a higher temperature, a decrease in the internal resistance increases the full charge capacity and voltage [22]. However, the

higher rate of the chemical activity (e.g., self-discharge) may reduce the actual capacity during storage at a high temperature. For both high and low temperatures, the further the operating temperature is away from the room temperature (e.g., 23°C), the quickly the battery will age. Reference [23] proposes the capacity as a function of the ambient temperature as follows.

$$Q_0 = Q_{0,25}[1 - \alpha(25 - T_a)] \tag{1-4}$$

where T_a is ambient temperature in °C, α is temperature coefficient, and Q_0 and $Q_{0,25}$ are the adjusted capacity at T_a and the nominal capacity at 25 °C in A-h, respectively. The coefficient α can be estimated by fitting the empirical data to (1-4).

An abnormally high internal temperature of a battery is a nearly universal warning of thermal runaway, which is a major fault in all batteries. These changes can occur within seconds, leading to a potentially catastrophic event. The internal temperature change of a battery can be estimated by the thermal energy balance equation [24].

$$m \cdot c_p \cdot \frac{dT(t)}{dt} = i(t)^2 R_{in} - h_c A[T(t) - T_a] \tag{1-5}$$

where m stands for the battery mass in kg, c_p is the specific heat in J/kg/K, R_{in} is the internal resistance, h_c is the heat transfer coefficient in W/m^2, A is the battery external surface area in m^2, and T_a is the ambient temperature in °C.

The heat power includes the resistive heat and the heat transferred to the environment. Additional heat generated from the entropy change or phase change and changes in the heat capacity can be ignored [24]. These omissions will not significantly affect the accuracy of battery models.

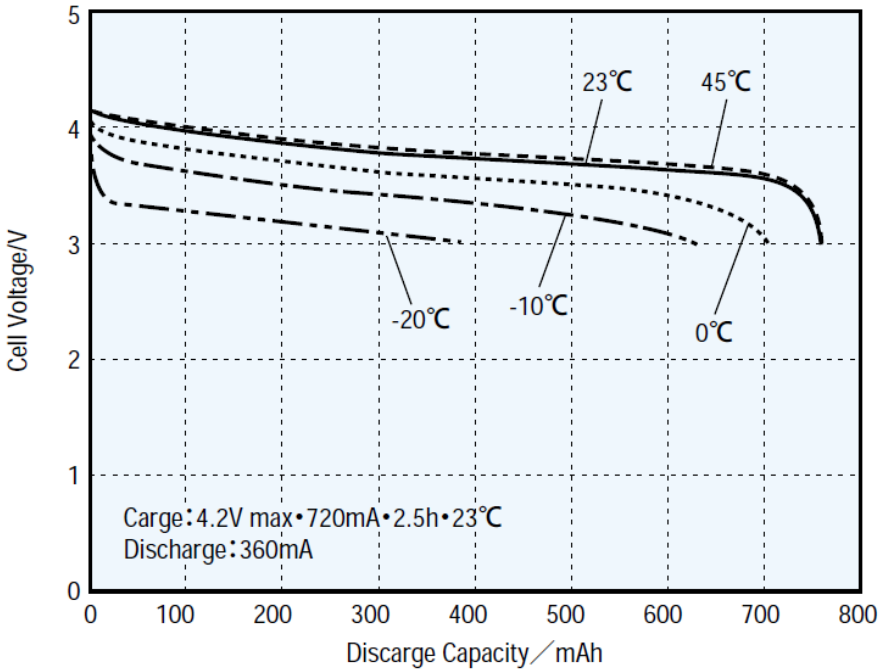

Figure 7. Changes in the discharge voltage of a polymer lithium-ion battery cell for a constant discharge current of 360 mA at ambient temperatures of -20°C, -10°C, 0°C, 23°C, and 45°C. (Courtesy of [17].)

1.2.6 Self-discharge

Self-discharge is a phenomenon in which a battery loses the stored charge due to unwanted chemical actions within the battery without any external connection. The self-discharge rate depends on the type of the battery, SOC, charge current rate, ambient temperature, etc. Figure 8 shows the change in discharge capacity retention for a fully charged lithium-ion battery stored at the ambient temperatures of 23° and 45°C, where the capacity retention of the battery prior to storage is 100% of the actual SOC. Figure 9 shows the battery capacity retention after long-term storage at a storage temperature of 45°C when the battery is initially in the fully-charged state, 50% charged state, and fully discharged state.

Typically, among rechargeable batteries, lithium batteries have the least amount of self-discharge around 2-3% discharge per month. The self-discharge of lead acid batteries is around 4-6% per month; while nickel-based batteries have higher self-discharge rates, e.g., 15–20% per month for nickel cadmium (NiCd) batteries and 30% per month for nickel metal hydride (NiMH) batteries [19], with the exception of low self-discharge (LSD) NiMH batteries, whose self-discharge rates are 2-3% per month [25].

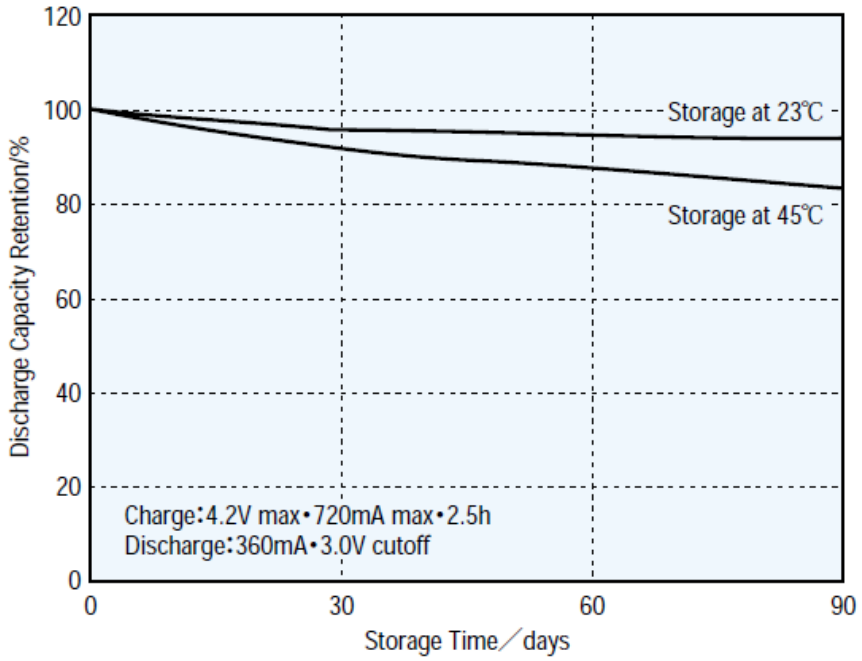

Figure 8. The change in discharge capacity retention for a fully charged battery stored at ambient temperatures of 23°C and 45°C, where the capacity retention of the battery prior to storage is 100%. (Courtesy of [17].)

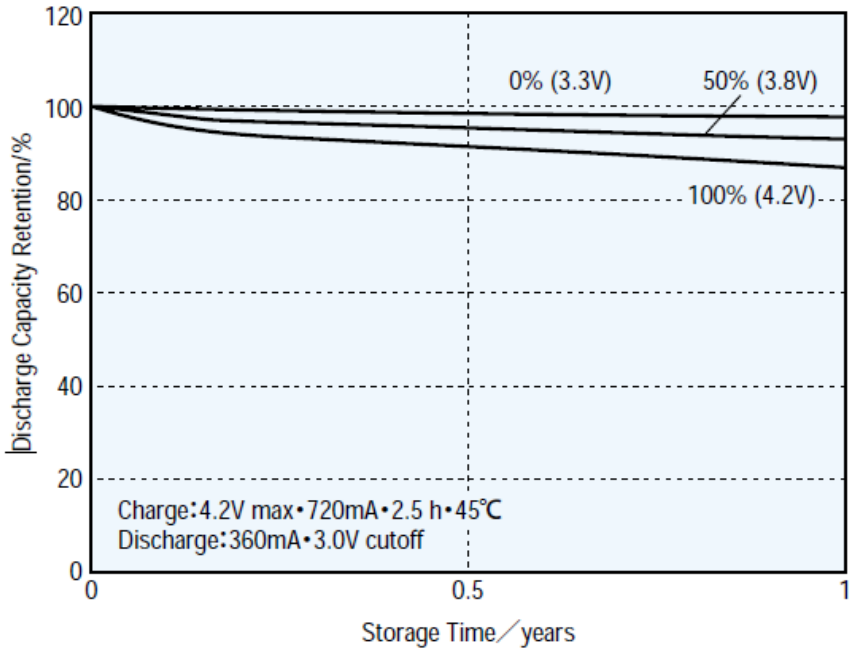

Figure 9. The battery capacity retention after long-term storage at a storage temperature of 45℃, when the battery is initially in the fully-charged state, 50% charged state, and fully discharged state. (Courtesy of [17].)

1.2.7 Aging Effect

A battery does not have infinite life time due to unwanted chemical reactions, including electrolyte decomposition, physical damage, and the loss of active materials in the battery. These irreversible changes usually cause unrecoverable capacity fade, and deteriorate the battery performance, such as increase of internal resistance and high self-discharge rate. These aging effects of the battery ultimately will result in battery failure. The aging process is caused by complex operating conditions affected by the number of cycling, ambient temperature, Depth of Discharge (DOD), current rate, etc. [26] The authors of [26] summarized the following:

a) High temperature accelerates the aging of the battery in both cycling and calendar modes;

b) Large DOD variance speeds up the aging process;

c) Arduous current cycle profile accelerates the aging process.

Figure 10 shows the charge/discharge cycle life characteristics when a lithium-ion battery is fully charged using CCCV, and then discharged using a constant current of 360 mA to a cutoff voltage of 3.0 V.

The State of Health (SOH) is an indicator of aging effect. SOH represents the capability of a battery to deliver the specified performance (e.g., capacity) compared with a new battery. SOH can be estimated by a single measurement of conductance or impedance of the battery cell, which is easy but inaccurate. Furthermore, battery parameters, such as capacity, internal resistance, self-discharge rate, charge acceptance, and discharge capabilities, can be used in a comprehensive way to improve the accuracy of the SOH estimation. In practice, SOH is defined as the ratio of the maximum charge capacity of an aged battery ($Q_{\text{max\_aged}}$) to that of a new battery ($Q_{\text{max\_new}}$) [27].

$$\text{SOH} = \frac{Q_{\text{max\_aged}}}{Q_{\text{max\_new}}} \tag{5}$$

Normally, a battery is said in the mild fault condition when the SOH of the battery is below 80%.

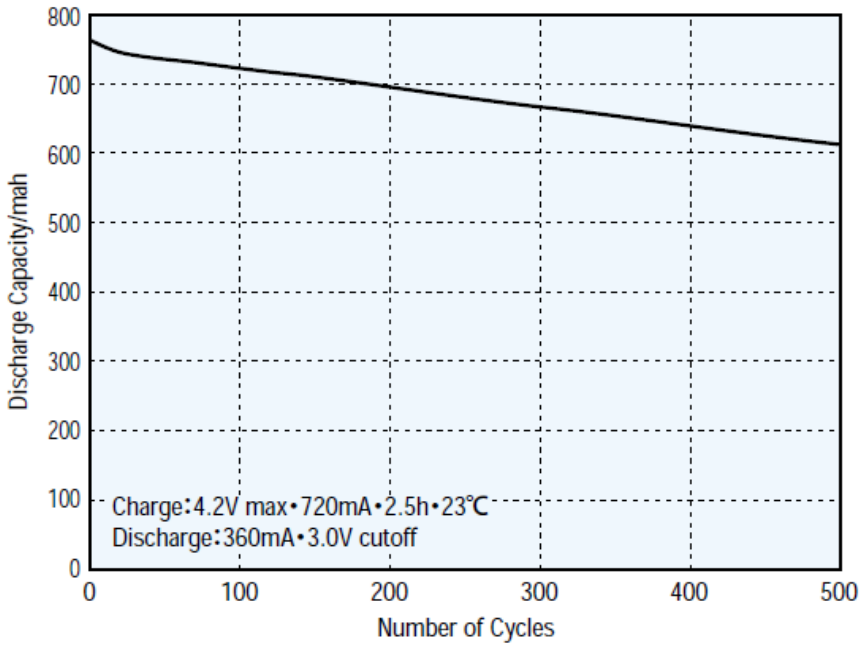

Figure 10. The charge/discharge cycle life characteristics when a lithium-ion battery is fully charged using CCCV, and then discharged using a constant current of 360 mA to a cutoff voltage of 3.0 V. (Courtesy of [17].)

1.2.8 Memory effect

Memory Effect is another manifestation of the changing morphology of NiCd battery cells with nonlinearity [19]. The battery remembers how much discharge was required on previous discharges and would only accept that amount of charge in subsequent charges, causing them to hold less charge than was expected. NiMH cells also have the memory effect but lesser than NiCd. In fact, the repeated shallow charges of a battery cell cause the crystalline structure of the electrodes to change as aforementioned, which causes the internal impedance of the cell to increase and its capacity to be reduced. Long slow charges, such as trickle charging, and high temperature tend to promote this undesirable crystal growth. However, the memory effect can be solved by the following process. To get the full charge, the battery should

be fully discharged before charging. Moreover, if the battery is allowed to do 3 to 5 cycles of charge/discharge, the battery capacity will be recovered.

1.3 Outline of Thesis

This thesis proposes a novel hybrid battery model based on an electrical circuit battery model and a Kinetic Battery Model (KiBaM) [28]. The KiBaM is capable of capturing nonlinear capacity effects, such as the recovery effect and rate capacity effect, for accurate SOC tracking and runtime prediction of the battery. Therefore, the proposed hybrid model can accurately capture dynamic electrical circuit characteristics and nonlinear behaviors of batteries for any operating conditions. The proposed model is effective for modeling any electrochemical batteries, such as the lead-acid, NiCd, NiMH, and lithium-ion batteries.

The outline of this thesis is the following:

Chapter 2 provides a literature review of different battery models, which are classified into five categories.

Chapter 3 describes the proposed hybrid battery model, followed by an explanation of nonlinear capacity variation and the method of parameter extraction.

Chapter 4 provides simulation and experimental results for single-cell and multicell lithium-ion batteries as well as a lead-acid battery to validate the proposed hybrid battery model.

Chapter 5 concludes the thesis and provides some discussions for future work.

Chapter 2: Literature Review

A variety of battery models have been developed for various purposes, such as battery design, performance estimation, prediction for real-time power management, and circuit simulation. In general, the existing battery models can be classified into five categories: electrochemical models, computational intelligence-based models, analytical models, stochastic models, and electrical circuit models.

2.1 Electrochemical Models

The electrochemical models use complex nonlinear differential equations to exactly describe chemical processes that take place in cells of batteries. For example, Doyle's electrochemical model consists of six coupled, nonlinear, differential equations [29]. These equations describe the dynamic voltage and current characteristics as functions of time, detailed physical reactions (e.g., the potentials), electrode phases, salt concentration, and reaction rate.

The DUALFOIL program uses this model to simulate lithium-ion batteries [30]. The program can be set by the users to compute the load profile as a sequence of constant current steps. The battery operating time is obtained by recording the time at which the battery voltage decreases below the cutoff voltage in discharge. The program has been extended to model other electrochemical battery models by including additional factors, such as energy balance and capacity fading [31].

The electrochemical models are the most accurate models. However, establishing these models requires detailed knowledge of the battery chemical processes, which makes

them difficult to configure [32]. Moreover, due to high complexity and intensive computation requirement, it is difficult to use these models for real-time battery power management and circuit simulation.

2.2 Computational Intelligence-Based Models

The computational intelligence-based models describe the nonlinear relationships among the quantities such as SOC, battery voltage, current, and temperature. ANN-based models [33], [34], support vector regression models [35], and mixed models have been used to estimate the battery nonlinear behaviors [36]. Recently, a recurrent neural network (RNN) has been used to provide an SOC observer and battery voltage estimator [34], as show in Figure 11. The RNN-battery model can accurately predict both the SOC and the terminal voltage of the batteries.

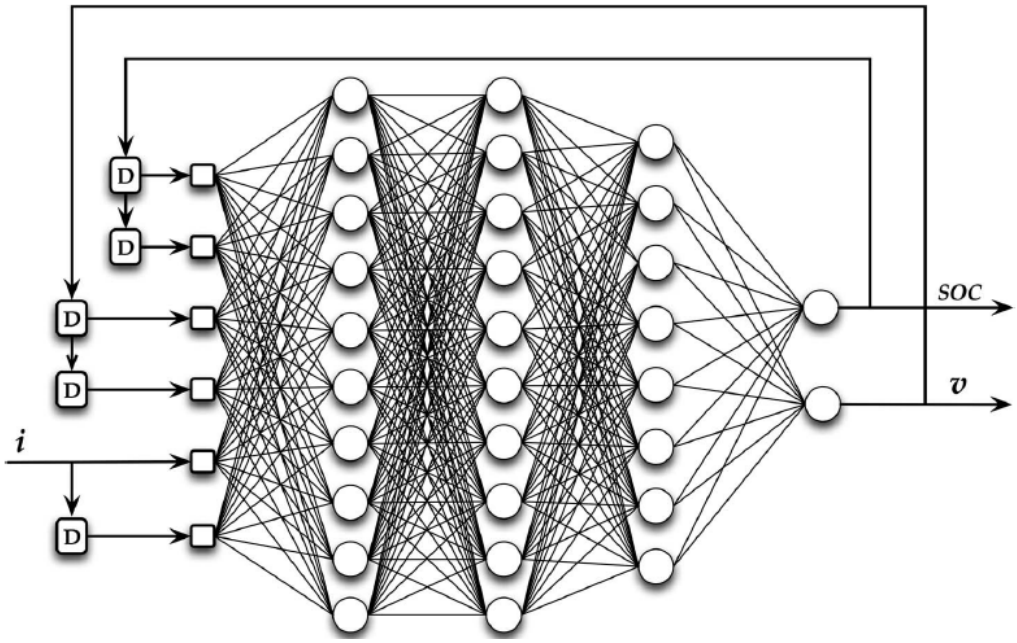

Figure 11. Recurrent Neural Network (RNN)-based battery model. (Courtesy of [34].)

Although accurate estimation of SOC and terminal voltage can be obtained by the computational intelligence-based battery models by including the nonlinearity of the batteries, the learning process required by these methods has a quite high computational cost.

2.3 Analytical Models

The analytical models are simplified electrochemical models that can capture nonlinear capacity effects and predict runtime of the batteries with reduced order of equations. These models perform well for SOC tracking and runtime prediction under specific discharge profiles. However, they cannot capture the dynamic current-voltage (I-V) characteristics of the battery required for codesign and cosimulation with other electrical circuits and systems.

2.3.1 Pueker's Law

The simplest analytical model is called the Peukert's law [37]. It captures the nonlinear relationship between the runtime of the battery and the rate of discharge, but the recovery effect is not taken into account. The nonlinear relationship can be written as:

$$C_P = LI^p \tag{2-1}$$

where C_p is the Puekert capacity in A-h, L is the battery lifetime, I is the discharge current, and p is the Puekert coefficient.

2.3.2 Kinetic Battery Model

Another analytical model is the KiBaM proposed in [28], [38]. The KiBaM is an intuitive and simple battery model, which was originally developed to model chemical processes of large lead-acid batteries by a kinetic process [28].

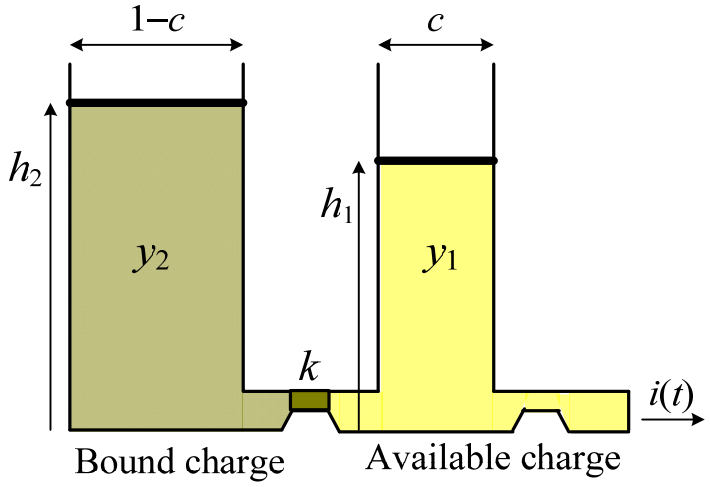

Figure 12. The Kinetic Battery Model (KiBaM).

The KiBaM describes the chemical processes of a battery by a kinetic process. It assumes that a battery has two charge wells, where the charge is distributed with a capacity ratio c ($0 < c < 1$) between the two wells, as shown in Figure. 12. The available charge well delivers charge directly to the load; while the bound charge well supplies charge only to the available charge well through a valve k. The rate of charge flows from the bound charge well to the available charge well depends on k and the difference in heights of the two wells, h_1 and h_2, where h_1 represents the SOC of the battery. The battery is fully discharged when h_1 becomes zero. The changes of the charges in the two wells are expressed as [32]:

$$\begin{cases} \dfrac{dy_1(t)}{dt} = -i(t) + k[h_2(t) - h_1(t)] \\ \dfrac{dy_2(t)}{dt} = -k[h_2(t) - h_1(t)] \end{cases} \tag{2-2}$$

where y_1 and y_2 are the total charges in the available charge well and the bound charge well, respectively; $h_1 = y_1/c$ and $h_2 = y_2/(1-c)$. When the battery is discharged with a current of $i(t)$, the available charge reduces faster than the bound charge and the difference in heights of the two wells grows. When the current is removed or reduced, the charge flows from the bound charge well to the available charge well until h_1 and h_2 are equal. Therefore, during an idle period or a small-current load, more charge becomes available effectively in the available charge well than when a large-current load is applied continuously. This explains both the recovery effect and rate capacity effect of the battery. Assume initial conditions of $y_{1,0} = y_1(t_0) = c \cdot C$, $y_{2,0} = y_2(t_0) = (1-c) \cdot C$, and $y_0 = y_{1,0} + y_{2,0}$, where C is the total battery capacity, the differential equations (2-2) can be

solved for a constant discharge current of I for a period of $t_0 \le t \le t_1$ by using Laplace transform; the solutions are given as:

$$\begin{cases} y_1(t) = y_{1,0}e^{-k'(t-t_0)} + \dfrac{(y_0k'c - I)[1 - e^{-k'(t-t_0)}]}{k'} \\ \qquad - \dfrac{Ic[k'(t-t_0) - 1 + e^{-k'(t-t_0)}]}{k'} \\ y_2(t) = y_{2,0}e^{-k'(t-t_0)} + y_0(1-c)[1 - e^{-k'(t-t_0)}] \\ \qquad - \dfrac{I(1-c)[k'(t-t_0) - 1 + e^{-k'(t-t_0)}]}{k'} \\ \delta(t) = h_2(t) - h_1(t) = \dfrac{y_2(t)}{1-c} - \dfrac{y_1(t)}{c}, \quad t_0 \le t \le t_1 \end{cases} \tag{2-3}$$

where k' (= k/[c(1–c)]) is a constant related to the diffusion rate; δ is the height difference between the two wells, which plays an important role in obtaining the nonlinear capacity variation. If the discharge current changes to a different value, y_1, y_2, and δ will be calculated by (2-3) with the new current value and initial conditions of $y_{1,0}$ and $y_{2,0}$, which are the final values of y_1 and y_2, respectively, for the previous discharge current. Therefore, (2-3) can be used to determine y_1, y_2, and δ for any continuous piecewise constant discharge currents. The discharge completes when y_1 becomes zero, indicating a zero SOC. Consequently, the unavailable charge, $u(t)$, of the battery can be expressed as follows [32]:

$$u(t) = (1-c)\delta(t) \tag{2-4}$$

2.3.3 Diffusion Model

The third analytical model is the diffusion model, which was developed to model lithium-ion batteries based on the diffusion of the ions in the electrolyte [39]. The model describes the evolution of the concentration of the electro-active species in the electrolyte to predict runtime under a given discharge load profile. This model is introduced by Fick's laws:

$$\begin{cases} -J(x,t) = D\dfrac{\partial C(x,t)}{\partial x} \\ \dfrac{\partial C(x,t)}{\partial x} = D\dfrac{\partial^2 C(x,t)}{\partial x^2} \end{cases} \tag{2-5}$$

where $C(x, t)$ is the concentration of species at time t and distant x from the electrode, J is the flux of the electro-active species at time t and distance x, and D is the diffusion coefficient. From the Fick's laws, the following analytical relationship between the battery current, lifetime, and parameter β can be used to calculate the apparent charge lost $\sigma(t)$ at time t .

$$\sigma(t) = \underbrace{\int_0^t i(\tau)d\tau}_{l(t)} + \underbrace{\int_0^t i(\tau)(2\sum_{m=1}^{\infty} e^{-\beta^2 m^2 (t-\tau)})d\tau}_{u(t)} \tag{2-6}$$

where the parameter β is related to battery recovery characteristics, and $l(t)$ and $u(t)$ are the dissipated charge to load and unavailable charge, respectively.

The KiBaM and the diffusion model take into account both the rate capacity effect and the recovery effect. However, they cannot describe I-V characteristics that are

important for electrical circuit simulation and multicell battery design. The KiBaM is actually a first-order approximation of the diffusion model [32].

2.4 Stochastic Models

The stochastic models [40]-[45] focus on modeling recovery effect and describes battery behavior as a Markov process with probabilities in terms of parameters that are related to the physical characteristics of an electrochemical cell. A stochastic KiBaM was developed to model a NiMH battery in [41] and [42], where the probability to recover during idle periods is made dependent on the length of the idle periods because the runtime of NiMH batteries strongly depends on the frequency of the load current. The stochastic battery model in [45] gives a good qualitative description for the behavior of a lithium-ion battery under pulsed discharge, as shown in Figure 13. The recovery effect is modeled as a decreasing exponential function of the SOC and discharge capacity. Assuming the discharge demand as a Bernoulli-driven stochastic process and Poisson distribution, respectively, the authors compare the result obtained from the electrochemical model of the lithium-ion cell and that derived from the stochastic model [46]. However, the model does not handle arbitrary load profiles with varying discharge currents and does not account for other battery nonlinearities.

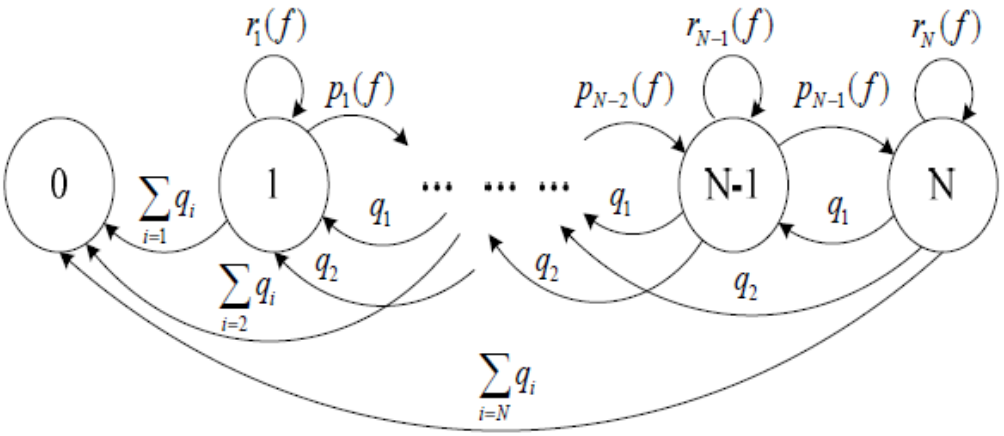

Figure 13. Stochastic process representing the cell behavior. (Courtesy of [45].)

In another paper [47], the authors extended the stochastic model in [45] to incorporate the rate capacity effect. The load is expressed as a stochastic demand on charge units. This model can account for both the rate capacity effect and charge recovery effect. Therefore, this model is relatively computational efficient and accurate to enable iterative battery life estimation for system level exploration. Both of the above models are based on the discrete time Markov chain construction.

2.5 Electrical Circuit Models

The electrical circuit models use equivalent electrical circuits to capture I-V characteristics and transient behavior of batteries by using combination of voltage and current sources, capacitors, inductors, and resistors. Some of these models can also track the SOC and predict the runtime of the batteries by using sensed currents and/or voltages. The electrical circuit models are good for codesign and cosimulation with other electrical circuits and systems.

The selection of electric component combination may depend on battery applications. In [48], the chemical processes inside batteries in the time domain are summarized and modeled. Figure 14 shows the major dynamic processes and their average time constants on which they operate.

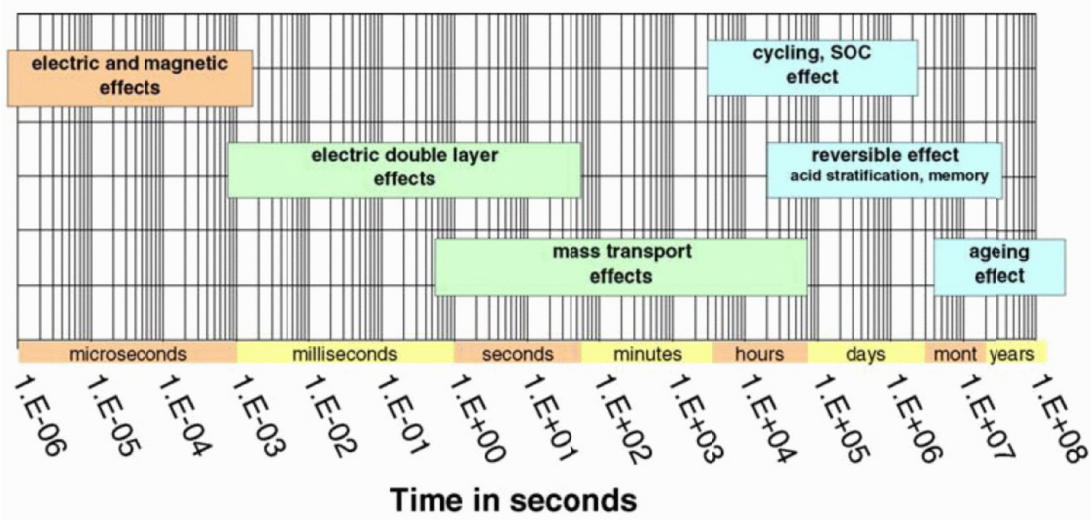

Figure 14. Major dynamic processes in batteries and their average time constants. (Courtesy of [48].)

These complex electrochemical processes can be expressed as impedances and divided into short-term and long-term processes. Short-term process includes electric, magnetic, electric double layer, and mass transport effect. Long-term process consists of cycling, SOC effect, reversible effect, and aging effect. The characteristic impedance of the battery can be observed by using Electrochemical Impedance Spectroscopy (EIS). An EIS instrument measures the potentials across a battery by applying small AC currents over a wide range of frequencies through a battery. The complex impedance of the battery is recorded and then, the EIS draws Nyquist plot that shows the complex impedance of the battery in a single curve over the entire frequency range. As for the short-term process, a

typical plot is shown in Figure 15 [48]. Its characteristics can be divided into three regions with respect to the frequency range. The low frequency region ranging from mHz to a few Hz shows mass transport (i.e., diffusion effect), which is similar to linear ohmic characteristics. A half circle in the middle range of a few Hz to kHz is similar to a RC parallel circuit and represents the charge transfer and electrochemical double layer effect. The high frequency range from kHz to MHz shows the conductance and skin effect, which is similar to inductor characteristics. An equivalent electrical network of the battery can be made based on this plot, as shown in Figure 16. Considering the electrolyte and electrode resistance (R_E), linear ohmic characteristics (R_w), charge transfer (R_{CT}), and electrochemical double layer effect (C_{DL}), Randle's equivalent circuit model can be used [14]. However, Randle's model is complex in simulation realization and it is hard to extract the parameters of the model [49].

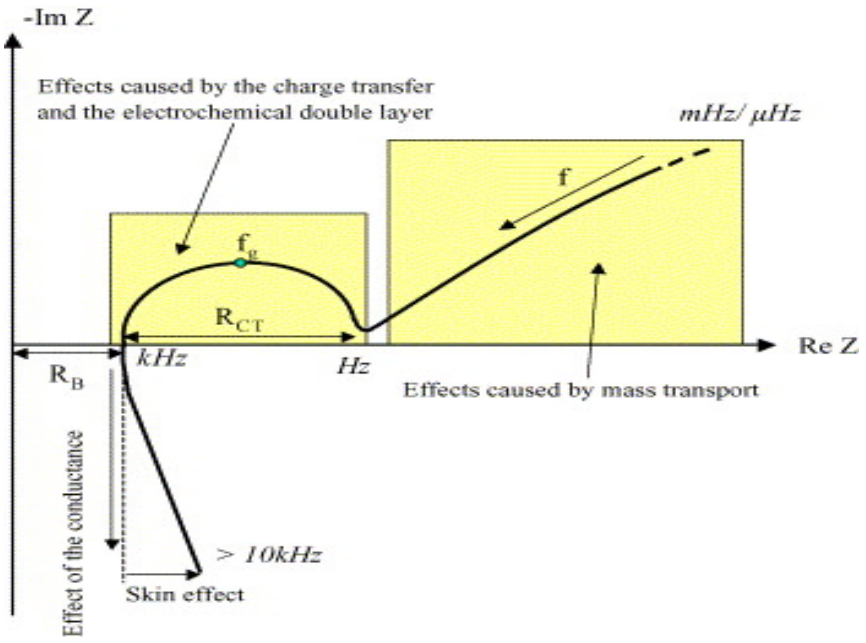

Figure 15. Typical Nyquist plot of a battery. (Courtesy of [48].)

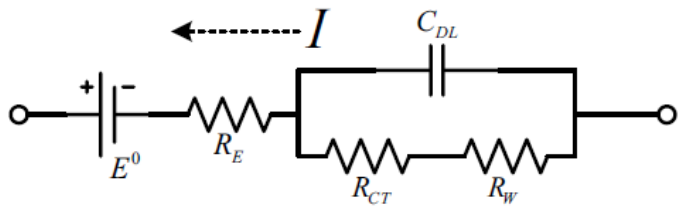

Figure 16. Randle's equivalent circuit model for a lithium-ion battery. . (Courtesy of [14].)

Figure 17 illustrates an electrical circuit model [50] for predicting battery run-time and I-V Characteristics for a single battery cell, which consists of two capacitor and resistor (RC) circuits. The RC circuit on the left is used for SOC tracking and runtime prediction for the battery cell, where the self-discharge resistance, $R_{\text{self-discharge}}$, is used to characterize the self-discharge energy loss of the battery cell; the capacitance, C_{capacity}, is used to represent the charge stored in the battery cell; the current source, i_{cell}, represents the charge/discharge current of the battery cell; the voltage across the capacitance, V_{SOC}, varies in the range of 0 V (i.e., the SOC is 0%) to 1 V (i.e., the SOC is 100%), representing the SOC of the battery cell quantitatively. The RC circuits on the right simulates the I-V characteristics and transient responses of the battery cell, where the voltage-controlled voltage source, $V_{\text{oc}}(V_{\text{SOC}})$, is used to bridge the SOC (i.e., V_{SOC}) to the open-circuit voltage, V_{oc}, of the battery cell; the series resistance, R_{series}, is used to characterize the charge/discharge energy losses of the battery cell; other resistances and capacitances are used to characterize the short-term (transient_S) transient responses, (e.g., the double layer capacitance and charge transfer), and long-term (transient_L) transient responses (e.g., equivalent to mass transport or diffusion process); and V_{cell} represents the terminal voltage of the battery cell.

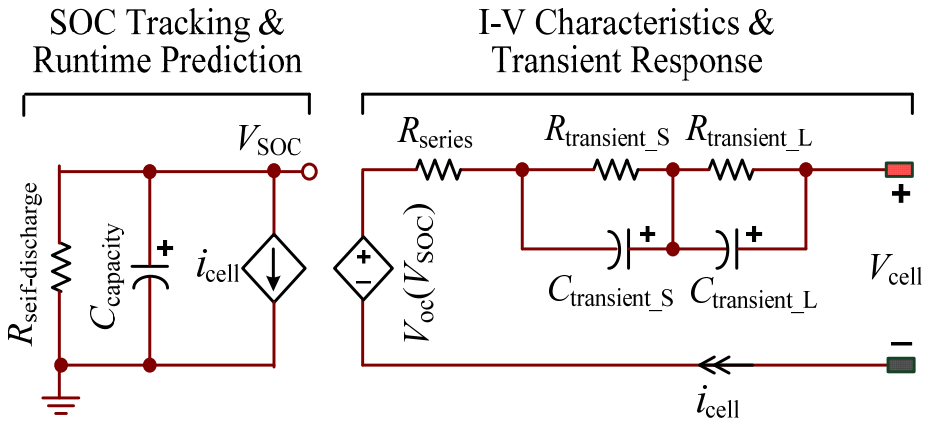

Figure 17. An electrical circuit battery model for predicting runtime and I-V characteristics.

The terminal voltage, V_{cell}, of the cell can be determined as follows by the open-circuit voltage, V_{oc}, and voltage drop due to the internal impedance Z_{eq} and current i_{cell} of Figure 17.

$$V_{cell} = V_{oc} - i_{cell} \cdot Z_{eq} \tag{2-7}$$

Other than using the left-hand-side RC circuit of Figure 17, the SOC can also be calculated as [51]:

$$SOC(t) = SOC_{initial} - \frac{\int i_{cell}(t)}{C_{usable}} \tag{2-8}$$

where $SOC_{initial}$ is the initial SOC the cell; C_{usable} is usable capacity of the cell. The open-circuit voltage and RC parameters of the model depend on the SOC [50].

The electrical circuit model is relatively accurate to capture the dynamic circuit characteristics of a battery cell, such as the open-circuit voltage, terminal voltage, transient response, and self-discharge. However, this model is unable to capture the nonlinear capacity behaviors, such as the rate capacity effect and recovery effect, of the battery due to the use of a constant capacitance, $C_{capacity}$, to represent the remaining usable

capacity of the battery. This reduces the model accuracy when predicting the battery performance at various load current conditions.

Recently, an enhanced circuit-based model was developed [52], [53] by mixing an RC electrical circuit model [50] with Rakhmatov's diffusion analytical model [39] to include the battery recovery effect. However, due to the high complexity of the diffusion analytical model, the enhanced model is highly complex and, therefore, is not feasible for real-time applications, such as real-time performance estimation/prediction for power management of batteries.

Chapter 3: The Proposed Hybrid Battery Model

3.1 The Proposed Hybrid Battery Model

The proposed hybrid model enhances the electrical circuit model in Figure 17 by replacing its left-hand-side RC circuit with an enhanced Coulomb counting algorithm based on the KiBaM to capture the nonlinear capacity variation of a battery, as shown in Figure 18. Therefore, the proposed model is capable of capturing comprehensive battery performance more accurately than the electrical circuit model in Figure 17 by coupling the dynamic electrical circuit characteristics with nonlinear capacity effects of the battery. In addition, the proposed battery model needs less computational cost than the enhanced model in [52], thereby is feasible for real-time applications.

Consider a period of $t_0 < t < t_r$ in which the battery cell is first discharged with a constant current (i.e., $i_{\text{cell}} = I > 0$) and then rests (i.e., $i_{\text{cell}} = 0$) for the remaining of the period. The proposed battery model is expressed by the following [54]:

$$SOC(t) = \frac{C_{available}(t)}{C_{\max}} = SOC_{initial} - \frac{[\int i_{cell}(t)dt + C_{unavailabl\ e}(t)]}{C_{\max}} \tag{3-1}$$

$$V_{oc}[SOC(t)] = a_0 e^{-a_1 SOC(t)} + a_2 + a_3 SOC(t) - a_4 SOC^{2}(t) + a_5 SOC^{3}(t) \tag{3-2}$$

$$V_{cell}(t) = V_{oc}[SOC(t)] - i_{cell}(t) \cdot R_{series} - V_{transient}(t) \tag{3-3}$$

$$V_{transient}(t) = V_{transient\_S}(t) + V_{transient\_L}(t) \tag{3-4}$$

$$V_{transient\_S}(t) = \begin{cases} R_{transient\_S} \cdot i_{cell}(t)[1 - e^{-(t-t_0)\tau_S}], & t_0 < t < t_d \\ V_{transient\_S}(t_d) \cdot e^{-(t-t_d)\tau_S}, & t_d < t < t_r \end{cases} \tag{3-5}$$

$$V_{transient\_L}(t) = \begin{cases} R_{transient\_L} \cdot i_{cell}(t)[1 - e^{-(t-t_0)\tau_L}], & t_0 < t < t_d \\ V_{transient\_L}(t_d) \cdot e^{-(t-t_d)\tau_L}, & t_d < t < t_r \end{cases} \tag{3-6}$$

where t_0, t_d, and t_r are the beginning time, discharge ending time, and (rest) ending time of the period, respectively; C_{max}, $C_{available}$, and $C_{unavailable}$ are the maximum, available, and unavailable capacities of the battery, respectively; $\tau_S = R_{transient\_S} \cdot C_{transient\_S}$; $\tau_L = R_{transient\_L} \cdot C_{transient\_L}$. The SOC of the battery reduces when it delivers charge to load, which is expressed by the enhanced Coulomb counting term in (3-1). The unavailable capacity, $C_{unavailable}$, represents the nonlinear SOC variation due to the nonlinear capacity effects of the battery. The initial SOC, $SOC_{initial}$, is the estimated SOC at the end of the last operating period before t_0. Therefore, to implement the proposed model, only the initial SOC at the beginning of the battery operation (i.e., $t = 0$) is needed. In practice, $SOC_{initial}$ can be corrected by using (3-2) with the open-circuit voltage measured during some resting time intervals of the battery cell to avoid the accumulation of SOC estimation errors of using (3-1). Moreover, if the battery operates in the charge mode, the current i_{cell} becomes negative, leading to the increase of the SOC when using (3-1).

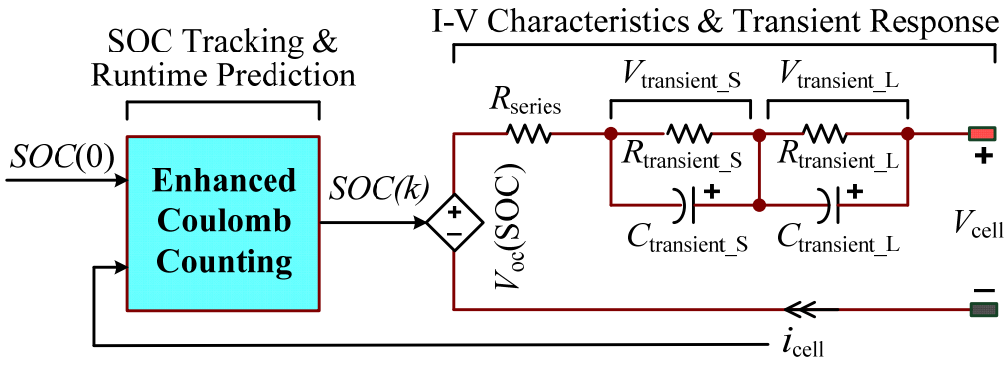

Figure 18. The proposed hybrid battery model.

As in (3-3), the terminal voltage, V_{cell}, is estimated by V_{oc}, the voltage across R_{series} (i.e., $i_{cell} \cdot R_{series}$), and the transient voltage term, $V_{transient}$, which represents the transient response of the RC network. The RC network parameters are functions of the SOC.

$$\begin{cases} R_{series}(SOC) = b_0 e^{-b_1 SOC} + b_2 + b_3 SOC - b_4 SOC^2 + b_5 SOC^3 \\ R_{transient\_S}(SOC) = c_0 e^{-c_1 SOC} + c_2 \\ C_{transient\_S}(SOC) = d_0 e^{-d_1 SOC} + d_2 \\ R_{transient\_L}(SOC) = e_0 e^{-e_1 SOC} + e_2 \\ C_{transient\_L}(SOC) = f_0 e^{-f_1 SOC} + f_2 \end{cases} \quad (3\text{-}7)$$

These parameters are approximately constant when the SOC is high (e.g., 20%-100% [50]) and change exponentially when the SOC varies below a certain value (e.g., 20%-0% [50]) due to the electrochemical reaction inside the battery. Equations (3-3)-(3-6) provide the time-domain response of the RC circuit in Figure 18.

3.2 Nonlinear Capacity Variation

The KiBaM is integrated into the proposed hybrid model to capture the capacity variation of the battery due to nonlinear capacity effects, such as the rate capacity effect

and recovery effect. The available capacity, $C_{\text{available}}$, which is the remaining usable capacity in the battery, is determined by:

$$C_{available}(t) = C_{initial} - l(t) - C_{unavailable}(t) \tag{3-8}$$

Where

$$l(t) = \int i_{cell}(t)dt \tag{3-9}$$

is the dissipated charge to load at the current of i_{cell} during the discharge period. The term $C_{\text{unavailable}}(t)$ of (3-8) represents the unavailable capacity at time t, which causes the available capacity to be smaller than the ideal value of $[C_{\text{initial}} - l(t)]$ due to the rate capacity effect. This effect can be interpreted by the KiBaM using the available and bound charges.

The unavailable capacity, $C_{\text{unavailable}}$, in (3-8) is determined by the unavailable charge, $u(t)$, obtained from the KiBaM model.

$$C_{unavailable}(t) = u(t) \tag{3-10}$$

A simplified expression for the unavailable charge $u(t)$ can be obtained from (2-3), given by the following equation.

$$u(t) = \begin{cases} (1-c)\cdot\left[\delta(t_0)e^{-k'(t-t_0)} + \dfrac{I}{c}\dfrac{1-e^{-k'(t-t_0)}}{k'}\right], & t_0 < t < t_d \\ (1-c)\cdot\delta(t_d)e^{-k'(t-t_0)}, & t_0 < t < t_d \end{cases} \tag{3-11}$$

During the discharge time interval ($t_0 < t < t_d$), u(t) increases, which represents the rate capacity effect. During the resting time interval ($t_d < t < t_r$), u(t) decreases because the charge flows from the bound charge well to the available charge well, which represents the recovery effect.

Based on (3-10) and (3-11), the unavailable capacity, $C_{\text{unavailable}}$, can be expressed by the following equation.

$$C_{unavailabl\ e}(t) = \begin{cases} C_{unavailabl\ e}(t_0)e^{-k'(t-t_0)} + (1-c)\dfrac{I}{c}\dfrac{1-e^{-k'(t-t_0)}}{k'}, & t_0 < t < t_d \\ C_{unavailabl\ e}(t_d)e^{-k'(t-t_d)}, & t_0 < t < t_d \end{cases} \quad (3\text{-}12)$$

where $C_{\text{unavailable}}$ (t_0) is zero at t_0= 0. The unavailable capacity determined by (3-12) enables the proposed model to capture the rate capacity effect during discharge and the recovery effect during rest of the battery. In general, if a battery is discharged with variable and discontinuous currents, then the entire discharge time can be divided into multiple periods and in each period the discharge current is constant or zero. Then (3-12) can be applied to each period to continuously capture the unavailable capacity of the battery. A special case is the discharge with a continuous constant current or with a constant pulse current.

Figure 19 shows the simulated nonlinear capacity variation of a 1-Ah, 3.7-V lithium-ion battery cell when it is discharged with a current of 3C (i.e., 3 A) for 500 seconds and then rests for 500 seconds with zero discharge current, where $k^{'}$ = 0.005 and c = 0.3 are used for the proposed battery model. In Figure 19, $C_{\text{unavailable}}$ increases over time during the discharge period and reaches the maximum value at time t_d = 500 seconds. After that, $C_{\text{unavailable}}$ reduces during the idle time from t_d = 500 seconds to t_r = 1,000 seconds, indicating that the unavailable capacity gradually becomes available, i.e., recovery of the battery capacity. The battery is fully discharged when $C_{\text{available}}$ becomes zero.

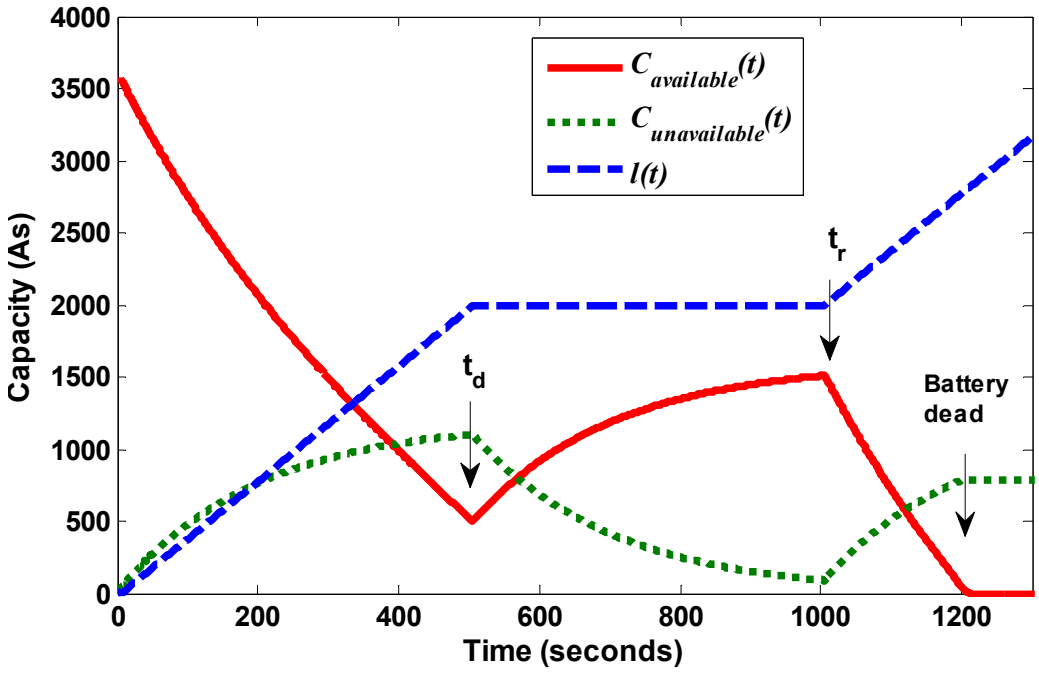

Figure 19. Nonlinear capacity variation of a 1-Ah lithium-ion battery cell when discharging with 3*C* for 500 seconds and resting for another 500 seconds.

Figure 20 shows the measured maximum available capacity of an 860-mAh, 3.7-V polymer lithium-ion battery cell (see Appendix), which depends on the discharge current. The extrapolating curve in Figure 20 illustrates the maximum available capacity at various load conditions. $C_{\text{unavailable}}$ increases as the discharge current increases, which results in the reduction of the available capacity. If the battery cell is discharged to an infinitesimal load, the battery runtime is extremely short. Therefore, there is no time for the charge to move from the bound charge well to the available charge well; the maximum available capacity equals the amount of charge in the available charge well. On the contrary, if the discharge current is small, all of the charges in the bound and available charge wells will become available to be delivered to the load.

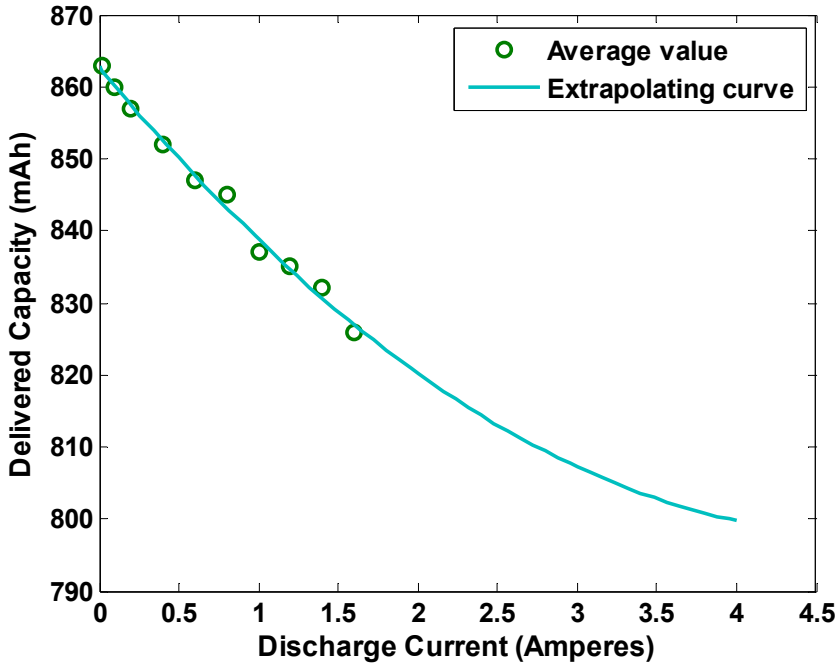

Figure 20. The maximum available capacity of an 860-mAh polymer lithium-ion battery cell as a function of the discharge current.

3.3 Model Extraction

All of the electrical circuit parameters of the proposed battery model can be extracted from least-square curve fitting of the experimental data obtained at room temperature using pulse discharge currents with an interval of 5% SOC. In this section, the 860-mAh, 3.7-V polymer lithium-ion battery cell will be used to illustrate how the model is extracted. The experimental procedure to extract V_{oc}(SOC) and R_{series} (SOC) is similar to that in [50], [55]. Figure 21 shows a typical curve of terminal voltage response used for extraction of the electrical circuit parameters of the proposed model. The battery cell is discharged with a current of I = 0.6C (i.e., 0.516 A) during $0 \le t \le t_d$ and then rests during $t_d \le t \le t_r$ with zero discharge current. During the time $0 \le t \le t_d$, 5 % SOC of the battery cell dissipated. Then, the battery cell rests for enough time, e.g., 30

minutes, to allow it to recover the unavailable capacity. This ensures that the electrical circuit parameters are independent of the rate capacity effect because the SOC tracking part of the model has taken into account that effect. V_{oc}(SOC) in (3-2) is extracted by estimating the steady-state open circuit voltage using exponential curve fitting. Moreover, the instantaneous voltage rising when discharge finished at t_d has relationship with R_{series}(SOC) in (3-13), which can be calculated by the following equation:

$$R_{series}(SOC) = \frac{V1 - V0}{I} \tag{3-13}$$

Based on (3-3)-(3-6), the following equation is obtained to estimate the RC network parameters:

$$V_{cell}(t) = a(1 - e^{-bt}) + c(1 - e^{-dt}) + e \tag{3-14}$$

where e is $V1$; $V_{cell} = V_{oc}$ when $t \to \infty$. The parameter a, b, c, and d are determined from the least-squares curve fitting. The RC network parameters can be then derived from (20).

$$\begin{aligned} R_{transient\_S} &= \frac{a}{I} \\ C_{transient\_S} &= \frac{1}{R_{transient\_S} \cdot b} \\ R_{transient\_L} &= \frac{c}{I} \\ C_{transientL} &= \frac{1}{R_{transient\_L} \cdot d} \end{aligned} \tag{3-15}$$

The parameter c and the initial conditions $y_{1,0}$ and $y_{2,0,}$ are determined from the maximum available charge (i.e., capacity Ah·3600 s) under very large and very small

current loads [42]. The delivered capacity under a very small current load is the total initial charge y_0 of the two charge wells. The maximum available capacity under a very large current load (i.e., the infinitesimal load) is the initial charge $y_{1,0}$ of the available charge well in Figure 12. Then the initial charge $y_{2,0}$ (= $y_0 - y_{1,0}$) of the bound charge well and the capacity ratio c (= $y_{1,0}/y_0$) can be determined. As shown in Figure 20, the maximum available charge is 3114 (= 0.865 Ah·3600 s), which is y_0; $y_{1,0}$ is 2872.8 (= 0.798 Ah·3600 s), where 0.798 Ah is the maximum available charge at the infinitesimal load. Consequently, the value of parameter c is 0.9248. The value of k' is determined in such a way that the unavailable capacity ($C_{\text{unavailable}}$) obtained from (3-12) agrees with experimental results by discharging the battery cell with continuous constant currents from the full SOC until the cutoff voltage is reached. Since $C_{\text{unavailable}}(t_0)$ is zero at $t_0 = 0$, t_d is known and the value of c has been derived, only k' is unknown in (3-12). Therefore, k' can be extracted. The parameter k' of the polymer lithium-ion battery cells is almost constant for any continuous current loads.

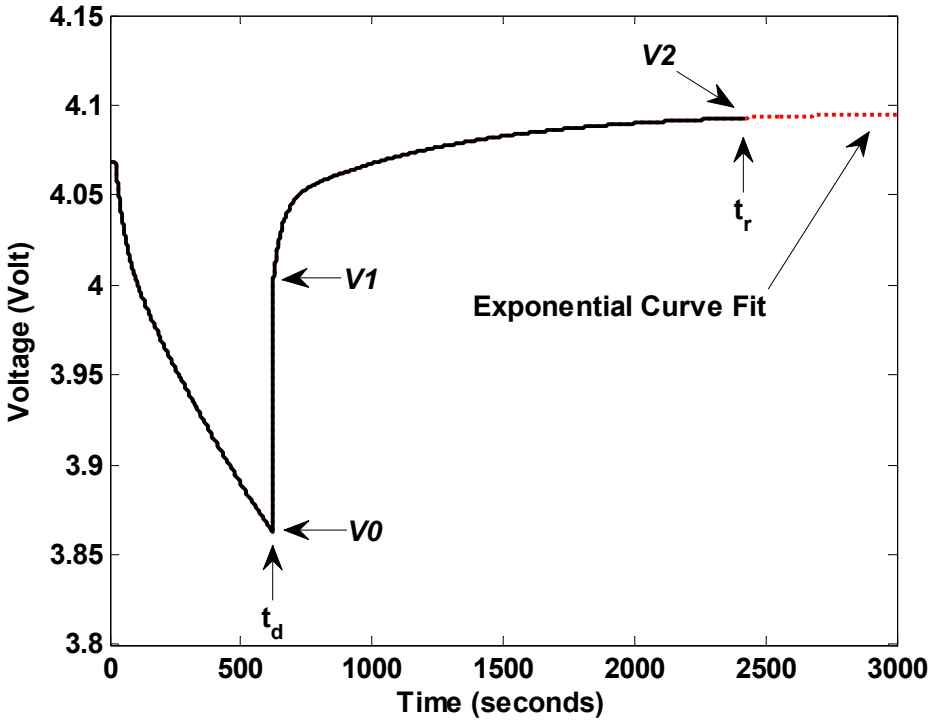

Figure 21. A typical curve of terminal voltage response under pulsed-current discharge for extraction of the electrical circuit parameters of the proposed battery model.

Chapter 4: Model Validation

Simulation and experimental studies are carried out to validate the proposed hybrid battery model for a single-cell as well as a six-cell polymer lithium-ion battery for various discharge current operations. Comparison with the electrical circuit model in [50] is also provided to show the superiority of the proposed model.

4.1 Simulation of the Proposed Battery Model

The proposed hybrid battery model is implemented in MATLAB/Simulink for an 860-mAh, 3.7-V polymer lithium-ion battery cell (see Appendix). The parameters of the single-cell model are obtained by using the model extraction method in Chapter 3 and are listed in Table 1. Based on the single-cell model, a series-connected, six-cell battery pack is built in MATLAB/Simulink. A cell switching circuit proposed in [51] and [56] is employed to control the operation (i.e., charge, discharge, and rest) of each cell independently. Figure 22 shows the implementation of the hybrid battery cell model in MATLAB/Simulink. The rated & recovery charge unit offers the nonlinear capacity variation by changing the value of $C_{\text{unavailable}}$ during battery operation. All circuit components are implemented by using the standard modules from the SimPower Systems toolbox.

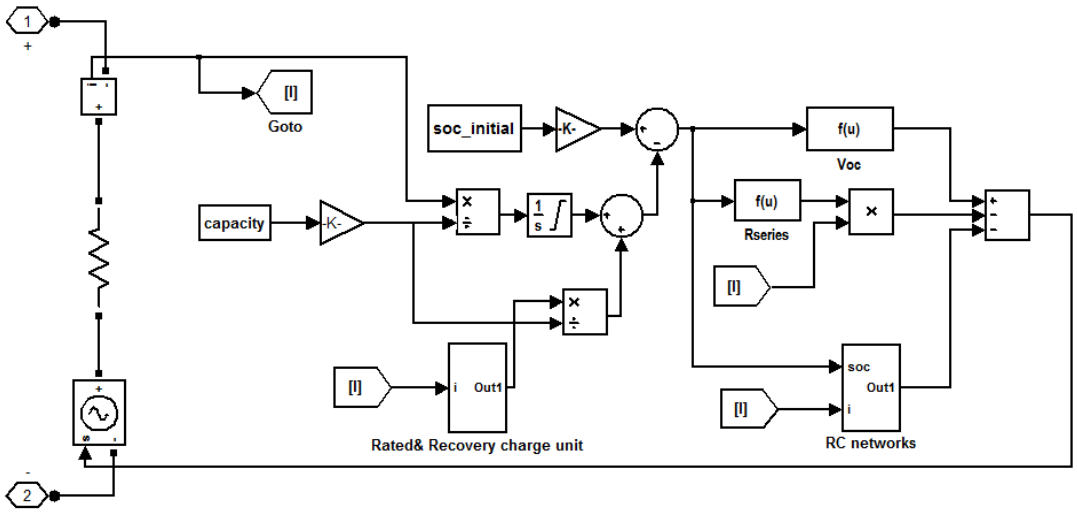

Figure 22. Hybrid single-cell battery model implemented in MATLAB/Simulink.

TABLE 1
BATTERY MODEL PARAMETERS FOR A POLYMER LITHIUM-ION CELL

a_0	-0.852	a_1	63.867	a_2	3.6297	a_3	0.559
a_4	0.51	a_5	0.508	b_0	0.1463	b_1	30.27
b_2	0.1037	b_3	0.0584	b_4	0.1747	b_5	0.1288
c_0	0.1063	c_1	62.49	c_2	0.0437	d_0	-200
d_1	-138	d_2	300	e_0	0.0712	e_1	61.4
e_2	0.0288	f_0	-3083	f_1	180	f_2	5088
$y_{1,0}$	2,863.3	$y_{2,0}$	232.66	c	0.9248	k'	0.0008

4.2 Experimental Setup

The six-cell battery pack simulated in MATLAB/Simulink is constructed in hardware to further validate the proposed model. Figure 23 illustrates the experimental setup. The cells are charged with CCCV by a DC source, and then discharged under

various discharge current profiles through a programmable DC electronic load, which offers Constant Resistor (C.R.), Constant Current (C.C.), and Pulsed Current (P.C.) modes as well as stores data such as current and voltage. High-efficiency power MOSFETs are used to construct the cell switching circuit on a printed circuit board (PCB) [51], [56]. The sensing, control and protection functions are also implemented on the PCB.

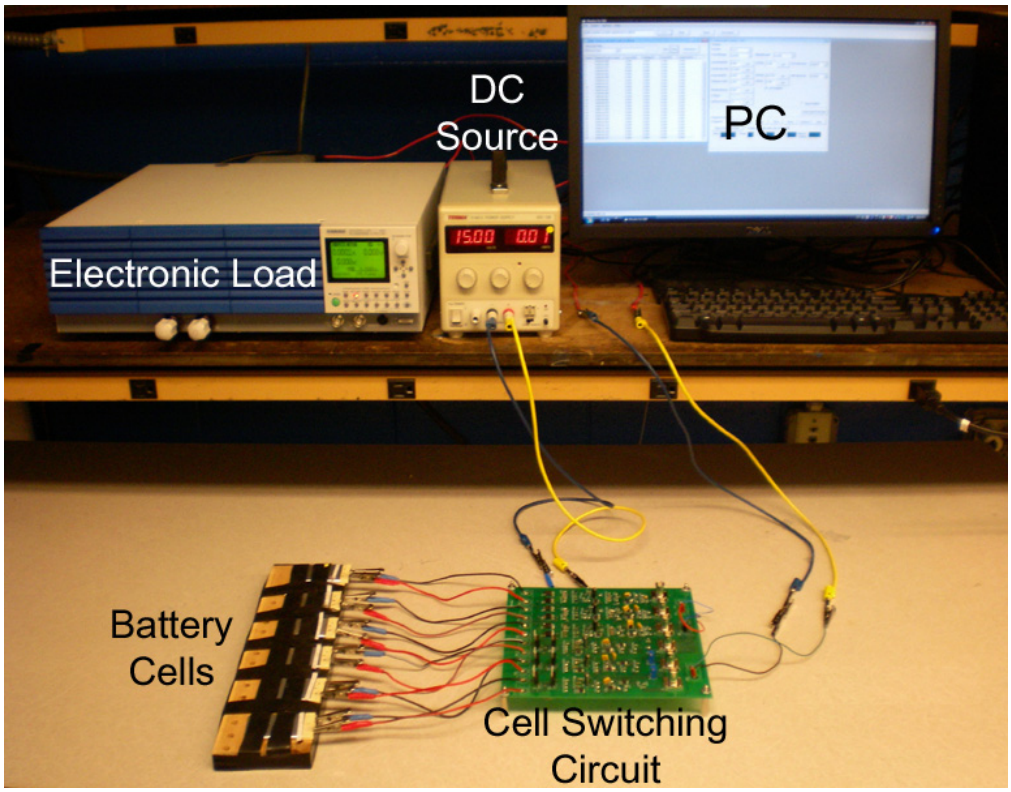

Figure 23. Experimental setup.

4.3 A Single Cell Study for Polymer Lithium-Ion Battery

Figure 24 compares the terminal voltage responses obtained from simulations using the electrical circuit model and the proposed hybrid model with experimental results for a single cell for two constant-current discharge scenarios, where the discharge

currents are 0.93C (0.8 A) and 1.86C (1.6 A), respectively. The terminal voltage responses obtained from the proposed model match the experimental results better than those obtained from the electrical circuit model, particularly when the battery cell is close to fully discharged. Therefore, the proposed model can accurately predict the runtimes of the battery cell under various discharge current conditions. However, due to neglecting the rate capacity effect, the runtime prediction errors of the electrical circuit model are obvious and increase significantly as the discharge current increases.

Figure 25 compares the terminal voltage responses obtained from simulations using the electrical circuit model and the proposed model with experimental results for two pulse-current discharge scenarios, where each current pulse has 600-second on time and 600-second off time. Again, the proposed model captures the dynamic responses and predicts the runtimes of the battery cell accurately under various pulse-current discharge conditions. On the other hand, due to neglecting the rate capacity and recovery effects, the errors of dynamic response tracking and runtime prediction of the electrical circuit model are larger than the proposed model and increase at higher discharge currents.

Furthermore, by capturing the variation of the unavailable capacity due to the recovery effect, the proposed hybrid model is able to accurately capture the SOC variation of the single cell under the pulse-current discharge, as shown in Figure 26.

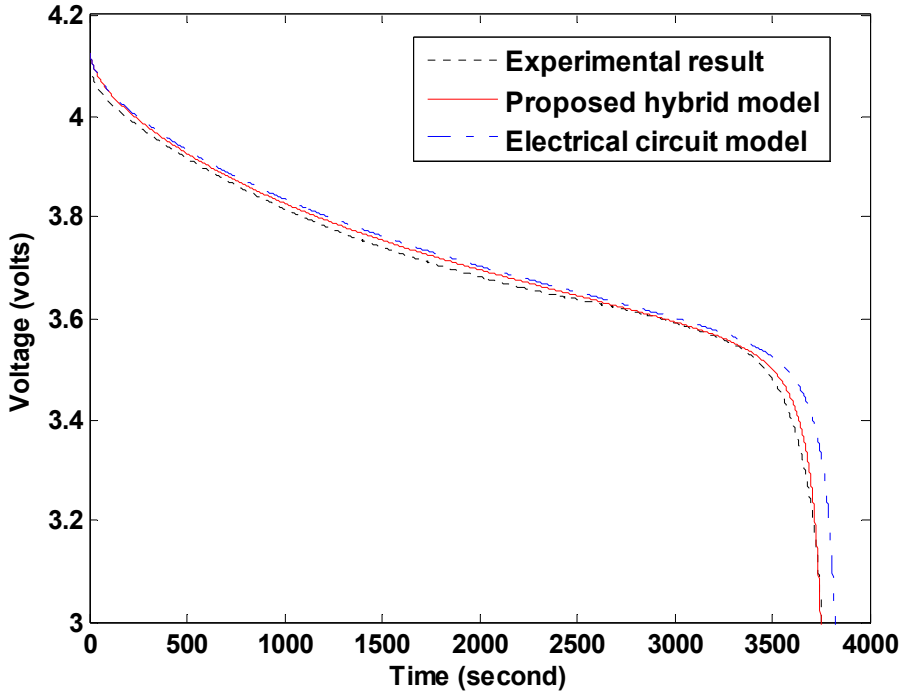

(a)

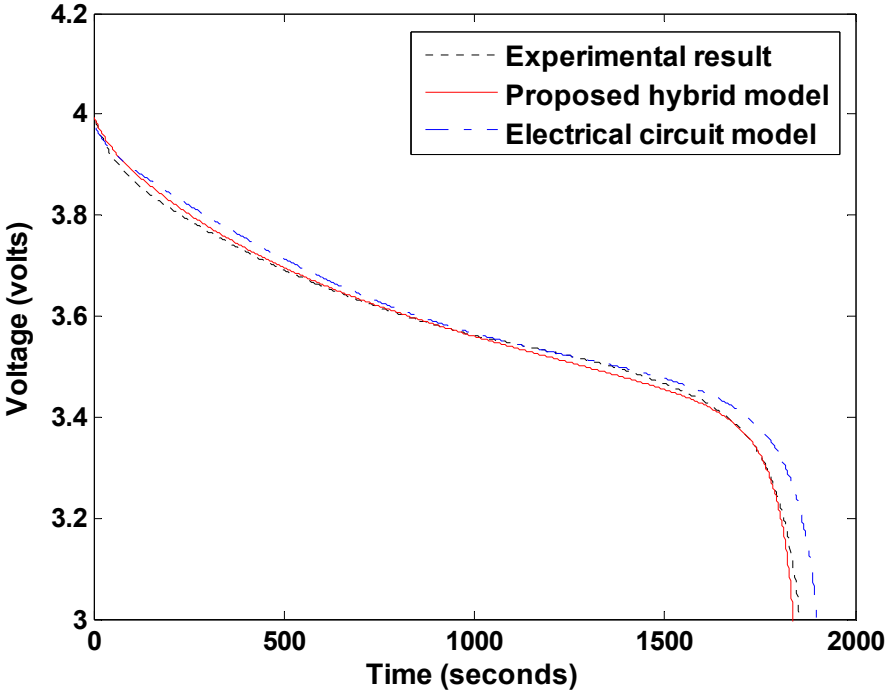

(b)

Figure 24. Comparison of simulation results of the electrical circuit model and the proposed hybrid model with experimental results for a single polymer lithium-ion cell with constant discharge currents of (a) 0.93C (0.8 A) and (b) 1.86C (1.6 A).

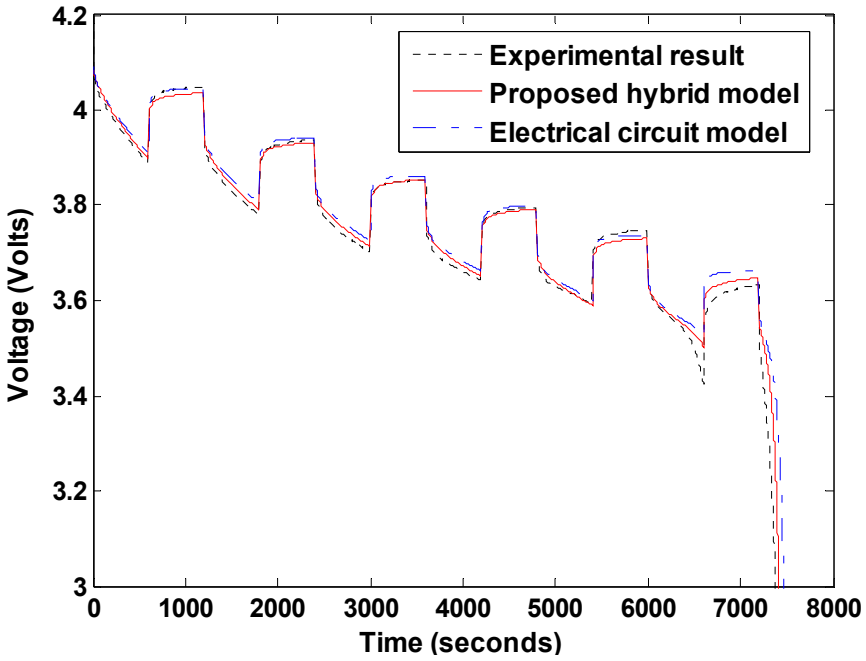

(a)

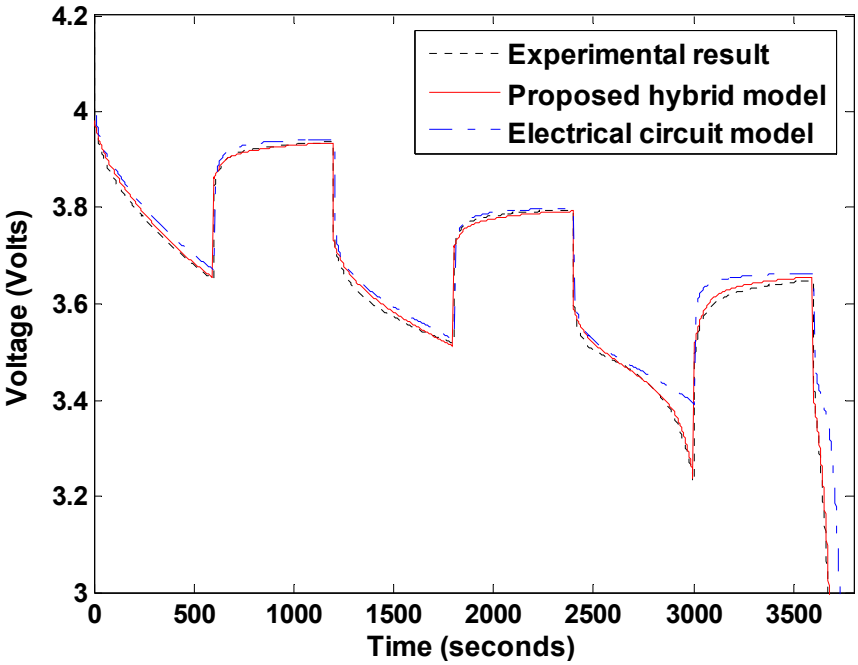

(b)

Figure 25. Comparison of simulation results of the electrical circuit model and the proposed hybrid model with experimental results for a single polymer lithium-ion cell with pulse discharge currents of (a) 0.93C (0.8 A) and (b) 1.86C (1.6 A), where each pulse has 600-second on time and 600-second off time.

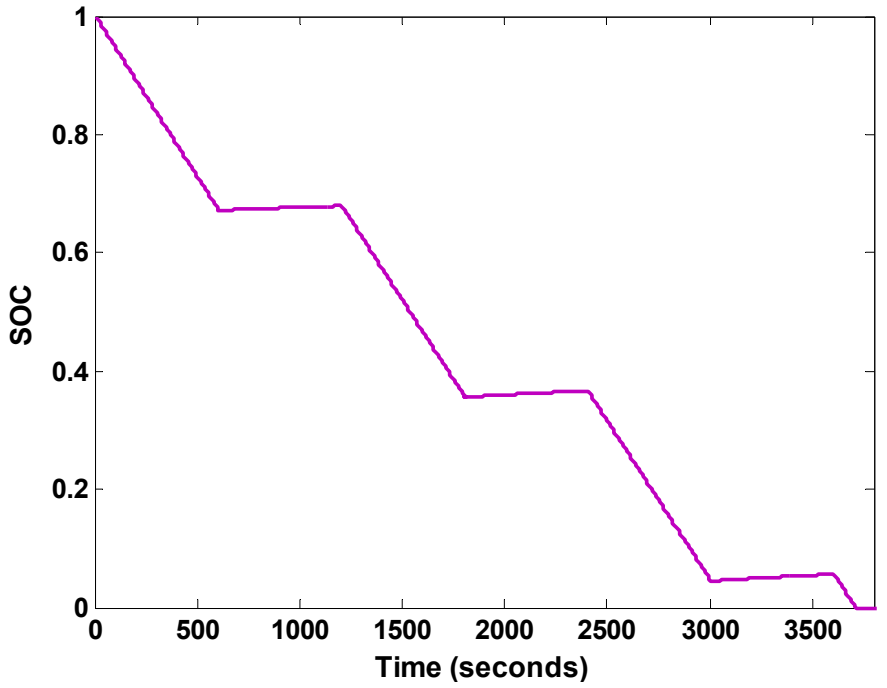

(a)

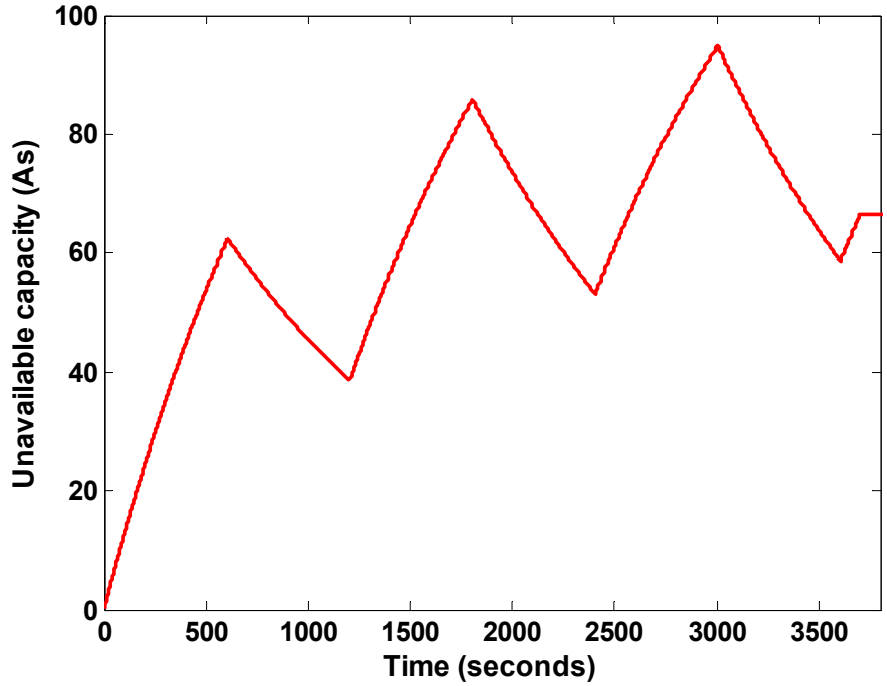

(b)

Figure 26. Nonlinear capacity variation estimated by the proposed model for a single polymer lithium-ion cell under a pulse discharge current of 1.86C (1.6 A), where each pulse has 600-second on time and 600-second off time: (a) SOC variation and (b) unavailable capacity.

4.4 A Multicell Study for Polymer Lithium-Ion Battery

Experiments are performed at different scenarios to compare with corresponding simulation results to validate the proposed battery model [56] for the six-cell polymer lithium-ion battery, where the dynamics of each cell are represented by the proposed model. For all scenarios, the experimental results agree with the simulation results obtained from the proposed model, as shown in Table 2. In Scenario 1, the six cells are discharged using the C.R. mode simultaneously. Since the initial SOCs of the cells are different, the cells are fully discharged sequentially. Once a cell is fully discharged, it will be disconnected from the battery pack by the cell switching circuit but the remaining cells still supply energy to the load. Figure 27 compares the terminal voltage responses of the six-cell battery obtained from simulation and experiment for Scenario 1. The results show that not only the steady-state but also the dynamic responses of the battery obtained from the simulation agree with those obtained from the experiment.

In Scenario 2, all of the six cells are discharged simultaneously using the C.C. method. In Scenario 3, the six cells are divided into two groups and each group has three cells. The two groups of cells are discharged alternatively, i.e., P.C. discharge, with a time interval of 300 s until all of the cells are fully discharged. Figure 28 shows that by using the cell switching circuit, the self-reconfigurable, six-cell battery provides energy to the load with the desired terminal voltage of ~12 V during operation. As shown in Table 2, compared to using the C.C. discharge (Scenario 2), more energy (300 mWh) is supplied by the six-cell battery when using the P.C. discharge (Scenario 3). This P.C. discharge method utilizes the recovery effect to improve the energy conversion efficiency of the multicell battery. These results show that proposed model can accurately capture the

nonlinear capacity variation and dynamic electrical circuit characteristics of each cell as well as the whole battery pack for various discharge modes.

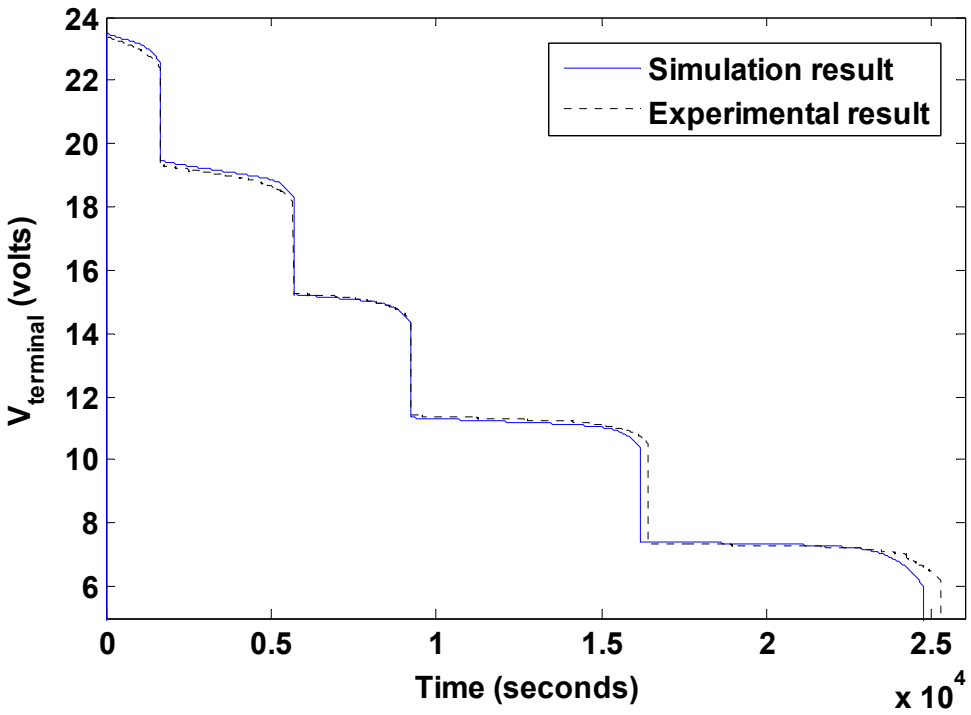

Figure 27. Comparison of simulation and experimental results in Scenario 1 for the terminal voltage of the six-cell battery.

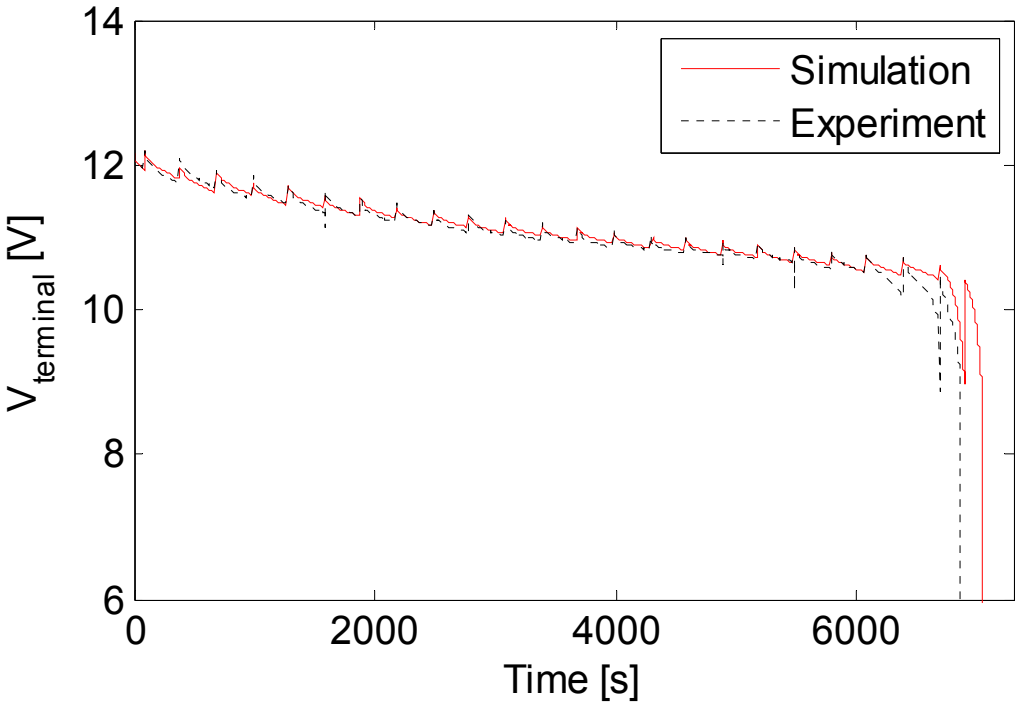

Figure 28. Comparison of simulation and experimental results in Scenario 3 for the terminal voltage of the battery.

TABLE 2
COMPARISON OF SIMULATION AND EXPERIMENTAL RESULTS FOR THE SIX-CELL BATTERY

Scenario	Discharge method	Initial cell conditions expressed by SOC [%]						Energy [Wh]	
		Cell 1	Cell 2	Cell 3	Cell 4	Cell 5	Cell 6	Simulation	Experiment
1	C.R. = 100 Ω	100	80	55	38	13	100	12.38	12.28
2	C.C. = 860 mA	100	100	100	100	100	100	18.41	18.30
3	P.C. = 860 mA (300s on, 300s off)	100	100	100	100	100	100	18.66	18.6

4. 5 A Study for Lead-Acid Battery

A lead-acid battery was tested to further validate the hybrid battery model. Table 3 shows the parameters of the battery model extracted by the method described in Chapter 3. The capacity ratio *c* of the lead-acid battery is lower than that of the polymer

lithium-ion cell; while k' of the lead-acid battery is higher than that of the lithium-ion cell. These parameters indicate that the lead-acid battery has higher nonlinear capacity variations than the lithium-ion battery.

Figure 29 compares the terminal voltage responses obtained from simulations using the electrical circuit model and the proposed hybrid model with the experimental result for a pulsed discharge scenario, where the battery is discharged with a constant current of 0.6C (0.74 A) for 40 minutes, rests for 30 minutes, and then discharged until the cutoff voltage is reached. As shown in Figure 29, the terminal voltage response obtained from the proposed model matches the experimental result much better than that obtained from the electrical circuit model. The errors of the terminal voltage predicted from the proposed model are less than 1% with respect to the experimental result. This means that the proposed model continuously tracks the SOC of the battery accurately. Consequently, the runtime of the battery predicted from the proposed model is almost the same as that obtained from the experiment. On the contrary, the error of the runtime predicted from the electrical circuit model is significant. Therefore, the proposed model can accurately capture the dynamic circuit characteristics and nonlinear capacity effects of lead-acid batteries as well.

TABLE 3
BATTERY MODEL PARAMETERS FOR A LEAD-ACID BATTERY

a_0	5.429	a_1	117.5	a_2	11.32	a_3	2.706
a_4	2.04	a_5	1.026	b_0	1.578	b_1	8.527
b_2	0.7808	b_3	-1.887	b_4	-2.404	b_5	-0.649
c_0	2.771	c_1	9.079	c_2	0.22	d_0	-2423
d_1	75.14	d_2	55	e_0	2.771	e_1	9.079
e_2	0.218	f_0	-1240	f_1	9.571	f_2	3100
$y_{1,0}$	2592	$y_{2,0}$	1728	c	0.6	k'	0.0034

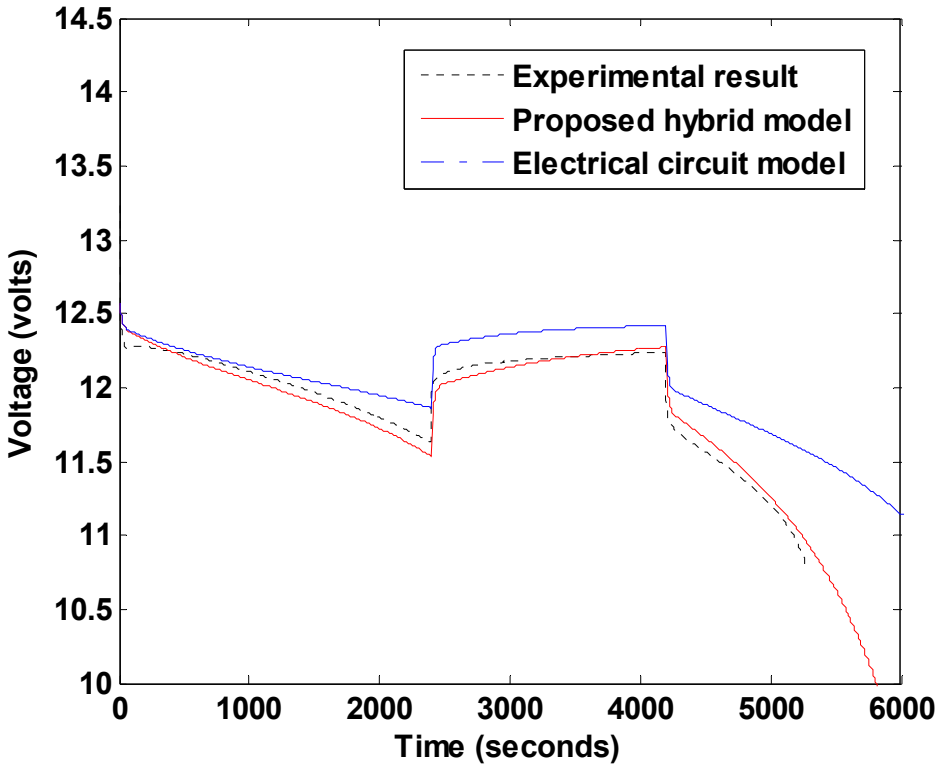

Figure 29. Comparison of simulation results of the electrical circuit model and the proposed hybrid model with experimental results for a lead-acid battery for a pulsed discharge scenario.

Chapter 5: Conclusions and Recommendations

This thesis has presented a novel hybrid battery model, which is capable of capturing dynamic electrical circuit characteristics and nonlinear capacity variation of battery cells under various operating conditions. The proposed battery model has been implemented in MATLAB/Simulink for a single-cell battery as well as a six-cell battery pack using 860-mAh, 3.7-V polymer lithium-ion cells and a 1.2 Ah, 12-V lead-acid battery. Simulation studies have been performed and compared with experiments to validate the proposed model. Results have shown that the proposed model is able to capture nonlinear capacity effects and dynamic electrical circuit characteristics and predict the runtimes accurately not only for single-cell but also for multicell batteries for various discharge modes and load current conditions. Compared to the existing electrical circuit battery models, the proposed hybrid model can offer more accurate SOC tracking and runtime prediction, thereby more accurate dynamic circuit characteristics capturing.

The proposed battery model can be applied to any type and size of electrochemical battery cells, such as lead-acid, NiCd, NiMH, and lithium-ion cells. It provides an accurate model for battery and circuit system designers to study various battery characteristics and optimally design battery systems for various applications. Moreover, the proposed battery model is computationally effective and can be used in battery power management to optimize the energy conversion efficiency and prolong the operating time of battery systems in real time.

In the future research, additional characteristics of rechargeable batteries, such as charging process, temperature effect, and aging effects, will be added to the proposed hybrid battery.

Bibliography

[1] Y. Çadırcı and Y, Özkazanç. "Microcontroller-based on-line state-of-charge estimator for sealed lead-acid batteries," *J. Power Sources,* vol. 129, pp. 330–342, 2004.

[2] W.X. Shen, K.T. Chau, and C.C. Chan, "Neural network-based residual capacity indicator for nickel-metal hydride batteries in electric vehicles," *IEEE Trans. Veh. Tech.*, vol. 54, no. 5, pp. 1705–1712, Sept. 2005.

[3] C. Bo, Z. Bai, and C. Binggang, "State of charge estimation based on evolutionary neural network," *Energy Convers. Manage.*, vol. 49, pp. 2788–2794, 2008.

[4] A.J. Salkind, C. Fennie, P. Singh, T. Atwater, and D.E. Reisner, "Determination of state-of-charge and state-of-health of batteries by fuzzy logic methodology," *J. Power Sources*, vol. 80, pp. 293–300, 1999.

[5] S. Malkhandi, "Fuzzy logic-based learning system and estimation of state of charge of lead-acid battery," *Eng. Appl. Artif. Intel*., 2006, 19, pp. 479–485.

[6] T. Hansen, and C. Wang, "Support vector based battery state of charge estimator," *J. Power Sources*, 2005, 141, pp. 351–358.

[7] X. Hu and F. Sun, "Fuzzy clustering based multi-model support vector regression state of charge estimator for lithium-ion battery of electric vehicle," in *Proc. Int. Conf. Intelligent Human-Machine Systems and Cybernetics*, Hangzhou, Zhejiang, China, 26–27 August.

[8] B.S Bhangu, P. Bentley, D.A. Stone, and C.M. Bingham, "Nonlinear observers for predicting state-of-charge and state-of-health of lead-acid batteries for hybrid-electric vehicles," *IEEE Trans. Veh. Tech*. 2005, 54, pp. 783–794.

[9] G.L. Plett, “Extended Kalman filtering for battery management systems of LiPB-based HEV battery packs-Part1: Background, Part2: Modeling and identification, Part3: State and parameter estimation,” *J. Power Sources*, 2004, *134*, pp. 252–292.

[10] A. Vasebi, S.M.T. Bathaee, and M. Partovibakhsh, “Predicting state of charge of lead-acid batteries for hybrid electric vehicles by extended Kalman filter,” *Energy Convers. Manage.* 2008, *49*, pp. 75–82.

[11] G.L. Plett, “Sigma-point Kalman filtering for battery management systems of LiPB-based HEV battery packs-Part 1: Introduction and state estimation, Part 2: Simultaneous state and parameter estimation,” *J. Power Sources*, 2006, 161, pp. 1356–1384.

[12] S. Jang, M. Shin, C. Yoon, and R. Campbell, “A study on adaptive autoreclosure scheme with real-time transient stability,” *J. Elect. Eng. & Technol.*, vol. 1, no. 1, pp. 8–15, 2006.

[13] M. Charkhgard and M. Farrokhi, “State of charge estimation for Lithium-ion batteries using neural networks and EKF,” *IEEE Trans. Industrial Electronics*, vol. 57, no. 12, pp. 4178 - 4187, Dec. 2010.

[14] W. Luo, C. Lu, L. Wang, and C. Liu, “Study on impedance model of Li-ion battery”, in *Proc. 6th IEEE Industrial Electronics and Application (ICIEA)*, 2011, pp.1943-1947.

[15] F. Zhang, Z. Shi, and W. Wolf, "A dynamic battery model for co-design in cyber-physical systems," in *Proc. 29th IEEE Int. Conf. Distributed Computing Workshops*, June 22-26, 2009, pp. 51-56.

[16] M. Doyle and J. S. Newman, "Analysis of capacity-rate data for lithium batteries using simplified models of the discharge process," *J. Applied Electrochem*., 27 pp. 846–856, July 1997.

[17] Sony, "Lithium Ion Rechargeable Batteries: Technical Handbook," Online. http://www.sony.com.cn/products/ed/battery/download.pdf

[18] T. L. Martin, "Balancing batteries, power, and performance: system issues in CPU speed-setting for mobile computing," Ph.D. dissertation, Carnegie Mellon University, Pittsburgh, Pennsylvania, 1999.

[19] Electropaedia web post: energy storage. Online. http://www.mpoweruk.com

[20] J. Li, E. Murphy, J. Winnick, and P. A. Kohl, "The effects of pulse charging on cycling characteristics of commercial lithium-ion batteries," *J. Power Sources*, vol. 102, no. 1–2, pp. 302–309, Dec. 2001.

[21] G. Yifeng, "Study on the fast charging method of lead-acid battery with negative pulse discharge," in *Proc. 4th Int. Conf. Power Electronics Systems and Applications (PESA 2011)*, 2011, pp.1-4.

[22] R. Rao, S. Vrudhula, and D. Rakhmatov, "Battery models for energy aware system design," *IEEE Computer*, vol. 36, pp. 1019-1030, Dec. 2003.

[23] H. Kim, "Dynamic Battery modeling in hybrid electric vehicles," Master thesis, The Ohio State University, 2002.

[24] D. Bernardi, E. Pawlikowski, and J. Newman, "A general energy balance for battery systems," *J. Electrochem. Soc*., vol. 132, no. 1, pp.5- 12, 1985

[25] SANYO, eneloop: LSD NiMH battery, Online. http://www.eneloop.info/home/general-description.html

[26] D. Haifeng, W. Xuezhe, and S. Zechang, "New SOH prediction concept for the power lithium-ion battery used on HEVs," in *Proc. 5th IEEE Veh. Power and Propuls. Conf.*, Dearborn, MI, USA, 2009, pp. 1649–1653.

[27] M. Coleman, C. K. Lee, and W. G. Hurley, "State of health determination: Two pulse load test for a VRLA battery," in *Proc. 37th IEEE Power Electron. Spec. Conf.*, 2006, pp. 1–6.

[28] J. Manwell and J. Mcgowan, "Extension of the kinetic battery model for wind/hybrid power system," in *Proc. 5th Eur. Wind Energy Assoc. Conf.*, 1994, pp. 1182–1187.

[29] M. Doyle, T. F. Fuller, and J. Newman, "Modeling of galvanostatic charge and discharge of the lithium/polymer/insertion cell," *J. Electrochem. Soc.*, vol. 140, no. 6, pp. 1526–1533, Jun. 1993.

[30] FORTRAN Programs for the Simulation of Electrochemical Systems. Online. http://www.cchem.berkeley.edu/jsngrp/fortran.html, June 2010.

[31] G.G. Botte, V.R. Subramanian, and R.E. White, "Mathematical modeling of secondary lithium batteries," *J. Electrochem. Acta*, vol. 45, pp. 2595–2609, May 2000.

[32] M. R. Jongerden and B. R. Haverkort, "Which battery model to use?," *IET Softw.*, vol. 3, no. 6, pp. 445–457, Dec. 2009.

[33] C.C. O'Gorman, D. Ingersoll, R.G. Jungst, T.L. Paez, "Artificial neural network simulation of battery performance", in *Proc. 31st Hawaii Int. Conf. System Sciences*, vol. 5, Jan. 1998, pp. 115-121.

[34] G. Capizzi, F. Bonanno, and G.M. Tina, "Recurrent neural network-based modeling and simulation of lead-acid batteries charge-discharge," *IEEE Trans. Energy Convers*., no. 99, pp. 1-9, 2011.

[35] J. Wang, Q. Chen, and B. Cao, "Support vector machine based battery model for electric vehicles," *Energy Convers. Manage*., vol. 47, pp. 858–864, 2006.

[36] W. X. Shen, C. C. Chan, E. W. C. Lo, and K. T. Chau, "Adaptive neuro-fuzzy modeling of battery residual capacity for electric vehicles," *IEEE Trans. Ind. Electron*., vol. 49, no. 3, pp. 677–684, Jun. 2002.

[37] D. Linden and T. Reddy, *Handbook of Batteries*, 3rd ed., McGraw-Hill, 2001.

[38] J. Manwell and J. Mcgowan, "Lead acid battery storage model for hybrid energy system," *Solar Energy*, vol. 50, pp. 399–405, 1993.

[39] D. Rakhmatov, S. Vrudhula, and A. Wallach, "An analytical high-level battery model for use in energy management of portable electronic systems," in *Proc. Int. Conf. Comput. Aided Design*, 2001, pp. 488–493.

[40] C. Chiasserini and R. Rao, "Pulsed battery discharge in communication devices," in *Proc. 5th Int. Conf. Mobile Comput. Netw*., 1999, pp. 88–95.

[41] K.M. Tsang, W.L. Chan, Y. K. Wong, AND L. Sun, "Lithium-ion Battery Models for Computer Simulation," in *Proc. IEEE Int Conf. Automation and Logistics (ICAL 2010)*, Aug. 2010, pp. 98-102.

[42] V. Rao, G. Singhal, A. Kumar, and N. Navet, "Battery modeling for embedded systems," in *Proc. 18th Int. Conf. VLSI Design*, 2005, pp. 105–110.

[43] C. Chiasserini and R. Rao, "A model for battery pulsed discharge with recovery effect," *in Proc. Wireless Commun. Netw. Conf*., 1999, pp. 636–639.

[44] C. Chiasserini and R. Rao, “Improving battery performance by using traffic shaping techniques,” *IEEE J. Sel. Areas Commun*., vol. 19, no. 7, pp. 1385–1394, Jul. 2001.

[45] C. Chiasserini and R. Rao, “Energy efficient battery management,” *IEEE J. Sel. Areas Commun*., vol. 19, no. 7, pp. 1235–1245, Jul. 2001.

[46] D. Panigrahi, C. Chiasserini, S. Dey, R. Rao, A. Raghunathan, and K. Lahiri, “Battery life estimation of mobile embedded systems,” in *Proc. Int. Conf. VLSI Design*, 2001, pp. 55–63.

[47] D. Panigrahi, C. Chiasserini, S. Dey, R. Rao, “Battery life estimation of mobile embedded systems,” in *Proc. 4th Int. Conf. VLSI Design*, pp.57–63, Jan 2001.

[48] A. Jossen, "Fundamentals of battery dynamics", *J. Power Sources*, vol. 154, no. 2, pp. 530-538, 2006.

[49] X. Gao, Z. Jun, and N. Ning, “Transient behavior modeling and physical meaning analysis for battery,” in *Proc. Int. Conf. Comp. Appl. and Sys. Modeling (ICCASM 2001)*, 2001, pp. 488–493.

[50] M. Chen and G. A. Rincon-Mora, “Accurate electrical battery model capable of predicting runtime and I-V performance,” *IEEE Trans. Energy Convers*., vol. 21, no. 2, pp. 504–511, Jun. 2006.

[51] T. Kim, W. Qiao, and L. Qu, “Series-connected reconfigurable multicell battery: A novel design toward smart batteries,” in Proc. *IEEE Energy Convers. Congr. Expo*., 2010, pp. 4257–4263.

[52] J. Zhang, S. Ci, Sharif, and M. Alahmad, “An Enhanced circuit-based model for single-cell battery,” in *Proc. 25th Appl. Power Electron. Conf. Exhib*., Feb. 2010, pp. 672–675.

[53] J. Zhang, S. Ci, Sharif, and M. Alahmad, "Modeling discharge behavior of multicell battery," *IEEE Trans. Energy Convers*., vol. 25, no. 4, pp. 1133–1141, Dec. 2010.

[54] T. Kim and W. Qiao, "A hybrid battery model capable of capturing dynamic circuit characteristics and nonlinear capacity effects," *IEEE Trans. Energy Conversion*, vol. 26, no. 4, pp. 1172-1180, Dec. 2011.

[55] S. Abu-Sharkh and D. Doerffel, "Rapid test and non-linear model characterization of solid-state lithium-ion batteries," *J. Power Sources*, vol. 130, pp. 266–274, 2004.

[56] T. Kim, W. Qiao, and L. Qu, "Series-connected self-reconfigurable multicell battery," in *Proc. 26th Appl. Power Electron. Conf. Expo*., Mar. 2011, pp. 1382–1387.

Appendix

The parameters of the polymer lithium-ion battery cells are listed as follows. Cell model: pl-383562 2C; nominal voltage: 3.7 V; nominal capacity: 860 mAh; discharge cutoff voltage (*Vcutoff*): 3 V; charge cutoff voltage (*Vover*): 4.2 V; maximum discharge current: 2C (1.72 A).

The parameters of the lead-acid battery are listed as follows. Battery model: LEOCH LP12-1.2AH; nominal voltage: 12 V; nominal capacity: 1.2 Ah; discharge cutoff voltage (V_{cutoff}): 10.8 V; charge cutoff voltage (V_{over}): 13.5 V; maximum discharge current: 15C (18 A).